



Published in final edited form as:

Neuron. 2020 December 23; 108(6): 1130–1145.e5. doi:10.1016/j.neuron.2020.09.033.

Wnt-Dependent Oligodendroglial-Endothelial Interactions Regulate White Matter Vascularization and Attenuate Injury

Manideep Chavali^{1,2,3}, Maria José Ulloa-Navas⁴, Pedro Pérez-Borredá⁴, Jose Manuel Garcia-Verdugo⁴, Patrick S. McQuillen¹, Eric J. Huang⁵, David H. Rowitch^{1,2,3,6,7,*}

¹Department of Pediatrics, UCSF, San Francisco, CA;

²Eli and Edythe Broad Institute for Stem Cell Research and Regeneration Medicine, UCSF, San Francisco, CA;

³New Born Brain Research Institute, UCSF, San Francisco, CA;

⁴Laboratorio de Neurobiología Comparada, Instituto Cavanilles, Universidad de Valencia, CIBERNED, TERCEL, Paterna, 46980, Spain.

⁵Department of Pathology, UCSF, San Francisco, CA;

⁶Department of Paediatrics and Wellcome-MRC Cambridge Stem Cell Institute, University of Cambridge, Hills Road, Cambridge, UK.

⁷Lead Contact.

SUMMARY

Recent studies have indicated oligodendroglial-vascular crosstalk during brain development, but the underlying mechanisms are incompletely understood. We report that oligodendrocyte precursor cells (OPCs) contact sprouting endothelial tip cells in mouse, ferret and human neonatal white matter. Using transgenic mice, we show that increased or decreased OPC density results in cognate changes in white matter vascular investment. Hypoxia promoted both increased OPC numbers and higher white matter vessel density, and endothelial cell expression of the Wnt pathway targets *Apcdd1* and *Axin2*, suggesting paracrine OPC-endothelial signaling. Conditional knockout of OPC *Wntless* resulted in diminished white matter vascular growth in normoxia, while loss of *Wnt7a/b* function blunted the angiogenic response to hypoxia resulting in severe white matter damage. These findings indicate that OPC-endothelial cell interactions regulate neonatal white

*Lead Author and Correspondence: David H. Rowitch MD PhD, Department of Paediatrics, University of Cambridge, Hills Road, Cambridge, UK, Tele: +44 01223 769386, dhr25@medschl.cam.ac.uk.

AUTHOR CONTRIBUTIONS

M.C. and D.H.R. conceived the original idea. M.C. designed and performed all experiments and data analysis. M.J.U.N. and J.M.G.V. performed Olig2 immunogold labelling and electron microscopy studies. P.P.B. performed surgical resection of the white matter tissue used for electron microscopy studies. P.S.M. and E.J.H. provided advice on experimental design related to ferret hypoxic injury and human HIE experiments respectively. M.C. and D.H.R. wrote the manuscript.

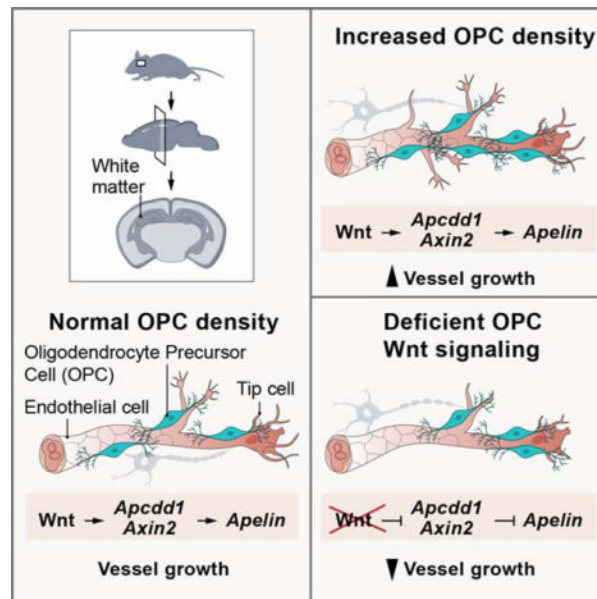
Publisher's Disclaimer: This is a PDF file of an unedited manuscript that has been accepted for publication. As a service to our customers we are providing this early version of the manuscript. The manuscript will undergo copyediting, typesetting, and review of the resulting proof before it is published in its final form. Please note that during the production process errors may be discovered which could affect the content, and all legal disclaimers that apply to the journal pertain.

DECLARATION OF INTERESTS

The authors declare no competing interests.

matter vascular development in a Wnt-dependent manner and further suggest this mechanism is important in attenuating hypoxic injury.

Graphical Abstract



eTOC Blurp

Chavali et al. demonstrate that oligodendroglial precursor density and their interactions with endothelial tip cells regulate development of white matter vasculature. In hypoxic brain injury, OPCs activate canonical Wnt signaling in angiogenic endothelial cells. Ablation of OPC-derived Wnt7 ligands results in disrupted white matter tip cell angiogenesis and myelination defects.

INTRODUCTION

Oligodendrocytes (OLs) are the myelinating cells of the central nervous system. During the process of myelination, developing oligodendrocyte precursors (OPCs) undergo dramatic changes in morphology and size as they differentiate, in some cases achieving a 7000-fold increase in membrane volume, to supply hundreds of myelin segments for nerve axons (Baron and Hoekstra, 2010; Webster, 1971). The consequent bioenergetic-requirements imply that the OPCs must have adequate access to a vascular network for nutrients, oxidative and metabolic substrates during myelination. Indeed, oligodendroglia intimately associate with the developing vasculature (Tsai et al., 2016; Yuen et al., 2014), and endothelial cells (EC's) have been shown to regulate myelination in development and disease (Niu et al., 2019; Rajani et al., 2018; Swire et al., 2019), suggesting bi-directional cell-cell interactions.

In the mammalian brain, angiogenesis commences at embryonic day 9 (E9), when superficial pial blood vessels (BVs) ingress into the deeper parenchyma (Greenberg and Jin, 2005; Plate, 1999; Vasudevan et al., 2008). By E10, a ventral periventricular plexus forms and starts to branch into the dorsal telencephalon to join the pial vessels (Vasudevan et al.,

2008). This network is refined via EC proliferation, sprouting, branching, vessel regression and stabilization (Carmeliet and Jain, 2011), processes regulated by local secretion of VEGF, BMPs, Wnts and axon guidance cues derived from various neural cell types (Adams and Eichmann, 2010; Carmeliet and Jain, 2011; Eichmann and Thomas, 2013). For example, neuroepithelial *Wnt7a/b* function has been shown to be essential for embryonic CNS vascular development (Cho et al., 2017a; Daneman et al., 2009; Stenman et al., 2008; Zhou et al., 2014).

The embryonic vasculature undergoes further remodeling in the postnatal and adult stages in a region dependent manner (Bozoyan et al., 2012; Harb et al., 2013). In this context, neuronal reelin regulates cortical vascular organization through activation of endothelial intrinsic Dab/ApoE signaling; disruption in this process results in neuronal positioning errors (Segarra et al., 2018). Adult neurogenesis and angiogenesis have also shown to be coupled in the germinal centers of brain, such as subventricular zone and subgranular zones (Le Magueresse et al., 2012; Shen et al., 2019; Tavazoie et al., 2008; Wang et al., 2019), where vascular-neural cell crosstalk regulates neuronal progeny generation and migration.

Here we show that OPCs physically interact with angiogenic tip cells in developing white matter (WM) and that these interactions are conserved in mouse, ferret and humans. To understand whether these interactions play a functional role in determining WM vascular structure, we used mouse transgenic lines to alter OPC numbers *in vivo* and observed a direct impact on WM vascular density. Neonatal hypoxic injury resulted in WM angiogenesis in ferret and human brain coupled to increased Wnt target gene expression in ECs. Genetic loss-of-Wnt ligand production in conditional *Wntless* or *Wnt7a/b* transgenic mouse OPCs caused a significant decrease in WM vascular investment, caused by decrease in sprouting angiogenesis and EC proliferation. We also observed that reduced WM vascular density led to a loss of mature OLs and hypomyelination, especially after hypoxic injury. Together, these results show that OPC-endothelial interactions are tightly coupled to ultimate vascular density in forebrain WM, and that OPC-derived Wnts attenuate susceptibility to hypoxic injury.

RESULTS

Evidence that OPCs physically interact with angiogenic tip cells in white matter.

Previous studies have indicated the importance of regional regulation of vascular development, metabolic activity and myelination (Harris and Attwell, 2012; Lam et al., 2010; Paredes et al., 2018). We first investigated the possibility that OPCs physically interact with sprouting endothelial tip cells. As shown (Figure 1A), such physical co-location was apparent through immunohistochemical analysis of P1 neonatal mouse brain with markers for OPCs (PDGFR α +Olig2+) and ECs (CD31+); three-dimensional reconstruction showed that OPC processes enwrap the sprouting tip cell filopodia (Figure 1A'). To compare OPC-tip cell proximity versus other glial cell types we used a transgenic *Sox10-GFP* OPC reporter (Kessaris et al., 2006) in conjunction with astroglial (GFAP+) and microglial (Iba1+) markers in P1 WM. We observed that OPCs made significantly more physical contacts than other glia. These contacts were also more complex around the tip cell filopodia, as compared to astrocytes and microglial cells (Figure 1B–D; Figure S1A).

Further, we found such OPC-endothelial tip cell interactions were conserved in developing ferret and human brain (Figure 1E–F; Figure S1B–D). Because angiogenic sprouting continues until the second postnatal week in mouse (Figure S1E), we investigated conservation by ultrastructural analysis of human two-year old resected subcortical WM tissue combined with Olig2 immunogold labelling (Figure 1G). We found that oligodendroglial cell (Olig2 immunogold+) processes formed similar physical contacts with nascent vessels with increased caveolae (Figure 1G–G'). The cell membrane at the OPC-contact site was also characterized by a lack of basement membrane, indicative of tip cell filopodia (Figure 1G'). These results suggest that OPC-endothelial tip cell physical interactions occur during the neonatal and postnatal WM development, a period during which active vascular network formation occurs.

Decreased OPC density is associated with white matter hypovascularization.

As we observed frequent OPC-endothelial tip cell interactions (Figure 2A), we asked if they had a functional significance on WM vascular development. To this end, we intercrossed several lines of transgenic mice to alter OPC numbers in the developing brain. To deplete OPC numbers, we generated *Olig2-cre*, *Sox10-lox-GFP-STOP-lox-DTA* (hereafter called *Sox10-DTA*), a transgenic line in which diphtheria toxin fragment A (DTA) falls under the transcriptional control of the *Sox10* promoter with toxic expression restricted to OPCs (Figure 2B; Figure S2A–B) (Kessaris et al., 2006). As shown in Figure 2C–E, we found a ~65% decrease in Olig2+ cell density in WM and cortical regions of *Sox10-DTA* mice at P1 compared to controls. Interestingly, we observed that WM vascular network was hypoplastic at this time point (Figure 2C–F).

While *Olig2-Cre* line targeted up to 75% of OPCs in the neonatal WM (Figure S2A), the cells that escaped Cre-targeting subsequently started to repopulate the brain (Figure S2B–C), and by P11 Olig2+ cell numbers had increased by ~15% (Figure 2G–I, Figure S2D). We therefore assessed the effect of OPC recovery on WM vascular development. As shown (Figure 2G–J), although there was a slight increase in Olig2+ cell numbers at P11, the vessel density, length and branching remained significantly lower than controls. Despite this, we did not detect abnormalities in blood brain barrier (BBB) structure/permeability, astrocyte endfeet coverage or microglial inflammatory response (Figure S2E–H). These findings indicated a positive correlation between oligodendroglial numbers and vascular density in WM (Figure 2K).

Increased oligodendroglial density results in white matter-specific hypervascularization.

We next tested if we could promote WM hypervascularization by bolstering OPC numbers. To achieve this, we intercrossed *Olig2-Cre* and *Braf^{V600E} (fl/+)* mice (Dankort et al., 2009) (constitutively active B-Raf; murine sarcoma viral oncogene homolog B, termed *BRAF^{CA}* hereon) (Figure 3A), a mitogenic driver for OPCs (Huillard et al., 2012). Analysis of *BRAF^{CA}* mice at P0 and P9 indicated a significant increase both in Olig2+ cell numbers and vessel density, branching and length in WM (Figure 3BI); this phenotype was sustained until P14, the extent of animal survival (Figure S3A–C). A recent study showed that tight perivascular clustering of OPCs on BVs in pathological conditions results in BBB damage (Niu et al., 2019). While OPCs in *BRAF^{CA}* mice did cluster on the vessels in the WM

(Figure 3J), we did not observe any disruptions in astrocyte endfeet coverage or BBB damage as assessed by unaltered PLVAP and Glut1/Claudin 5 expression in vessels and more importantly, absence of low molecular weight cadaverine leakage into brain parenchyma (Figure 3K–N; Figure S3D). Together, these results indicated that increased OPC numbers directly correlated with density of the WM vascular network (Figure 3O).

To determine whether OPC density also affected BV coverage in gray matter, we analyzed motor and somatosensory cortex from *Sox10-DTA* and *BRAF^{CA}* animals. Although the oligodendroglial cell density was significantly decreased at both P1 and P11 in *Sox10-DTA* cortex, no corresponding decreases in vascular density were noted in these regions (Figure S4A–C). Similarly, while oligodendroglial cell density was significantly increased in *BRAF^{CA}* cortex at both P0 and P9, we did not detect any vascular density increase in these regions (Figure S4D–F). These results indicate that oligodendroglial density induced vascular network formation is WM-specific.

Chronic hypoxic injury acutely increases OPC density and white matter vascular investment in ferret and human neonatal brain.

To assess pathophysiological relevance of such OPC-vascular interactions in WM, we first tested a ferret chronic sublethal hypoxia model (Figure 4A). As shown (Figure 4B), chronic exposure of neonatal kits to mild hypoxia (10% FiO₂) from P10–P20 resulted in hypomyelination consistent with previous reports (Tao et al., 2012). We found that hypoxia caused a significant increase in numbers of immature PDGFRa+Olig2+ OPCs in WM tracts with reduced numbers of more mature BCAS1+Olig2+ premyelinating cells (Fard et al., 2017) (Figure 4C–D, F). Interestingly, as shown (Figure 4E, F), we also observed a significant increase in vascular density accompanied by higher vessel length and branching in the WM tracts of hypoxia reared ferret kits.

Human neonatal hypoxic-ischemic encephalopathy (HIE) causes neuronal cell death, gliosis and WM injury (Figure S5A) (Billiards et al., 2008; Kinney and Back, 1998; Liu and McCullough, 2013; Northington et al., 2011)^{26,39}. We analyzed WM tracts from six cases of HIE and age matched controls (Figure 4G; Table S1). Intriguingly, histological analysis of vascular markers showed a significantly increased vessel density and branching in WM tracts of HIE cases (Figure 4H, I). Furthermore, we also found an increase in immature OPCs (PDGFRa+Olig2+) (Figure 4J, M) and reduced numbers of both premyelinating (BCAS1+Olig2+) and myelinating (Nogo-A+Olig2+) OLs in HIE (Figure 4K–M). We found no alterations in vascular junctional marker Claudin 5, indicating vascular integrity was not disrupted (Figure S5B). Together, these results suggest that systemic hypoxia-ischemia results in positively correlated acutely increased WM OPC and vascular densities (Figure 4N).

Endothelial Wnt signaling target gene upregulation in human HIE.

Histological analysis of human neonatal brain revealed that OPC proximity to BVs coincided with increased expression of the Wnt signaling downstream target Lef1 in ECs (Figure S5C). As OPCs make physical contacts with angiogenic vessels and given that Wnts are short range signals that can induce downstream activation in neighboring cells (Figure

40) (Clevers et al., 2014), we further assessed human HIE cases and controls for evidence of active OPC-driven Wnt signaling in ECs by immunohistochemistry and single molecule fluorescent *in situ* hybridization (smFISH). As shown (Figure 4P, Figure S5D–E), we detected that OPCs expressed *WNT7A* mRNA, encoding an angiogenic Wnt, in HIE lesions. We next assessed expression of the Wnt transcriptional targets *Apccdd1* and *Axin2* in CD31+ ECs in HIE lesions and observed a significant increase in their transcripts (Figure 4Q–R). In line with these results, we also observed an increase in Lef1+ ECs in WM tracts of HIE cases as well as hypoxic ferret brain (Figure S5F–H). Together, these findings suggest that Wnt ligand activity in human OPCs results in paracrine activation of Wnt/ β -catenin target gene activation in ECs of WM affected by hypoxic injury.

OPC-encoded *Wntless* function is essential for neonatal white matter vessel development.

As increased WM vascular density in human HIE lesions was coupled with Wnt target gene expression in endothelia, we next asked if OPC-encoded Wnt ligands play a functional role in WM vascular development *in vivo*. To this end, we generated OPC conditional knockout of *Wntless* (Carpenter et al., 2010), a transmembrane protein required for Wnt family trafficking and secretion (Banziger et al., 2006) (Figure 5A–B). At P3, conditional knockout of *Wntless* in OPCs (hereafter, *Wntless* cKO) did not result in WM abnormalities (Figure 5C–D; Figure S6A); however, by P7 the WM vascular density started to deteriorate and was significantly reduced by P12 (Figure 5E–J). Oligodendroglial cell numbers remained unaltered at P7 in *Wntless* cKO WM, but their numbers declined significantly by P12 (Figure 5E–F, H–I). These findings indicated a functional requirement for OPC-derived Wnt cues.

Canonical Wnt signaling is essential for BBB maturation (Daneman et al., 2009; Stenman et al., 2008). To understand if Wnt production from OPCs is needed for BBB integrity, we analyzed small molecular weight cadaverine leakage in *Wntless* cKO animals; we found no abnormalities in cortex or corpus callosum (Figure 5K–L). Similarly, we did not detect any fibrinogen deposits in brain parenchyma (Figure 5M) or, alterations in expression of the genes, *Plvap*, *Cldn5*, *Zic3*, *Foxf2* and *Mfsd2a*, involved in BBB maturation and maintenance in WM tissue isolates obtained from P8–P10 mice (Figure 5N), or major alterations in the EC junctional integrity as indicated by PLVAP, Glut1 and Claudin 5 protein expression in WM vessels (Figure S6B). We observed a minor increase in GFAP+ astrocyte reactivity, but not significant changes in activated Iba1+ microglial cell numbers or morphology (Figure S6C). These findings indicate that BBB integrity is maintained in *Wntless* cKO animals.

OPC-encoded *Wntless* function is essential for neonatal white matter sprouting angiogenesis and vessel growth.

We asked if disruptions in *Wntless* cKO WM vascular development were the result of deficient neonatal sprouting angiogenesis. We analyzed the developing WM vessels at P7. As shown (Figure 6A–B), although numbers of sprouting tip cells were unaltered, we observed a significant decrease in tip cell filopodial length, a finding consistent with previous studies that have shown that decreased angiogenesis is often associated with disruptions in tip cell filopodial development (Fantin et al., 2015).

To understand if the tip cell developmental phenotype was a result of disruptions in known genetic programs, we analyzed candidate tip cell marker and pro-angiogenic gene expression in WM tissue isolates by qPCR. Expression of genes, Vascular endothelial growth factor receptor 2 (*Vegfr2*), Notch ligand and Delta like 4 (*Dll4*) and most other pro-angiogenic cues were unaltered (Figure 6C, D). In contrast, we observed significantly decreased expression of Apelin (*Apln*) (Figure 6C). Apelin expression in endothelial tip cells is known to activate its receptor (APJ) in stalk cells thereby regulating proliferation and vessel growth (del Toro et al., 2010; Kidoya and Takakura, 2012).

To quantify expression of *Apln* at a single cell level we performed smFISH. As shown (Figure 6E–F), *Apln* expression in WM endothelial tip cells of *Wntless* cKO animals was significantly decreased at P7 and P12 along with *Axin2* (Figure 6F). To further resolve the involvement of canonical Wnt signaling, we quantified Wnt downstream targets *Apcdd1* and *Axin2* in CD31+ ECs and observed a significant decrease in these transcripts (Figure 6G–H). Moreover, we also observed a decline in WM EC proliferation in *Wntless* cKO animals. These findings suggest that OPC-specific loss of Wnt ligand production results in down regulation of *Apln* and decreased vessel growth through disrupted sprouting angiogenesis and EC proliferation (Figure 6I–J).

OPC-encoded *Wntless* is required for white matter integrity.

Because we found a decrease in Olig2+ cell numbers in the WM region of *Wntless* cKO animals, we analyzed if this was due to oligodendroglial cell proliferation defects; however, we found no differences in Olig2+Ki67+ cell numbers at P12 (Figure S6D) or alterations in expression of canonical Wnt downstream targets *Axin2* (Figure 7A) or TCF4 (Figure S6E). In contrast, we found a significant increase of apoptotic marker cl-caspase 3 in MBP+ OLs at P7 in both WM and deep cortical regions (Figure 7B). At P12, we found significantly decreased numbers of mature CC1+ and *Plp1*+ OL numbers (Figure 7C–F), resulting in WM hypomyelination (Figure 7G). We also observed that *Wntless* cKO progressively displayed tremors, hind limb clasping and reduced viability after second postnatal week (Video S1). Analysis of WM at P18 (extent of survival) also revealed appearance of axonal damage marker SMI32 and APP+ axonal spheroids (Figure 7H–I). These findings suggest a model in which OPC-encoded *Wntless* function is essential for WM vascularization, OL survival, postnatal myelination and ultimately WM integrity.

OPC-encoded *Wnt7a/b* function attenuates white matter injury post-hypoxia.

We and others have reported roles for *Wnt7a/b* in regulating embryonic and postnatal CNS developmental angiogenesis (Cho et al., 2017b; Cho et al., 2019; Daneman et al., 2009; Stenman et al., 2008; Yuen et al., 2014; Zhou and Nathans, 2014). To determine whether OPC-encoded *Wnt7a/b* function was essential during development or conferred resilience against hypoxic injury, we generated a compound *Wnt7a/b*-deficient mutant mouse by intercrossing *Olig2-Cre* to conventional *Wnt7a* null and conditional *Wnt7b* (*fl/fl*) alleles (hereafter *Wnt7dKO*) (Figure 8A), resulting in a significant decrease in *Wnt7* ligand expression in oligodendroglial cells (Figure 8B).

Given that *Wnt7dKO* mice showed improved survival and only subtle developmental impact in WM versus *Wntless* cKO mice, we tested the effects of superimposed chronic neonatal hypoxemia (Hx) in *Wnt7dKO* mutant mice and controls (Figure 8C). As shown (Figure 8D–E), wildtype mice reared in hypoxic conditions (10% FiO₂; Hx) showed the expected angiogenic response resulting in increased WM vascular density and branching. In dramatic contrast, this response and EC proliferation were lacking in hypoxic *Wnt7dKO* mice (Figure S7A–B). We confirmed the downregulation of Wnt downstream targets *Apccdd1* and *Axin2* in these mutants (Figure S7C–D) and did not observe BBB disruption (absence of PLVAP protein expression changes and no cadaverine leakage) or gliosis in hypoxic *Wnt7dKO* mutants versus controls (Figure S7E–G). Of note, *Wnt7a*^{-/-} conventional or *Olig2-Cre/Wnt7b (fl/fl)* conditional single mutants did not show a detectable phenotype post-hypoxic insult (Figure S7H–I). We conclude that combined function of OPC-*Wnt7a/b* is critical for the hypoxia-induced WM angiogenic response.

As we observed a significant decrease in both oligodendroglial and vessel density in P11 hypoxic reared *Wnt7dKO* mutants (Figure 8D, F), we investigated the timing of this decline. At P7, hypoxic reared *Wnt7dKO* mice began to show vascular density deterioration while oligodendroglial cell density remained unchanged (Figure S8A–B). Similar to results above with *Wntless* cKO animals, we observed increased apoptosis in WM of hypoxic *Wnt7dKO* mutants as well as reduction in CC1+ and *Plp1*+ mature OLs, severe hypomyelination, increased expression of axonal damage marker SMI32 and reduced WM volume (Figure 8G–M; Figure S8C). In contrast to WM, cortical oligodendroglial and OPC numbers remained unchanged (Figure S8D–E). Together, these findings indicate that OPC-encoded *Wnt7* function is a critical determinant of WM susceptibility to hypoxic injury. They do not exclude roles for other OPC-encoded Wnt ligands or other OPC-derived angiogenic factors in regulation of developmental WM angiogenesis in normoxic or hypoxic conditions.

DISCUSSION

Here we addressed the fundamental question of how vascular density is orchestrated in mammalian cortical WM and implications of this for resilience against hypoxic insult in neonatal brain. A major insight is that OPC-endothelial tip cell interactions play a direct role in this process and that alterations in OPC density and angiogenic signaling drive vascular remodeling in WM. We show that oligodendroglial-EC interactions attenuate susceptibility to hypoxic neonatal brain injury in a Wnt-dependent manner, a finding with implications for human neonatal WM injury, cerebral palsy and WM stroke. These and other findings discussed below indicate bi-directional crosstalk between OPCs and vasculature during development and in disease.

Evidence for OPC-endothelial bi-directional crosstalk in white matter.

Vascular investment of primordial brain regions depends on neuroepithelial and radial glial angiogenic cues including canonical Wnt signaling (Grutzendler et al., 2014; Lam et al., 2010; Ma et al., 2013; Stenman et al., 2008). The embryonic vasculature is subsequently remodeled at neonatal stages by neuronal and glial populations (Bozoyan et al., 2012; Harb et al., 2013; Ma et al., 2013; Paredes et al., 2018; Segarra et al., 2018; Vasudevan et al.,

2008), including NG2 glia (Minocha et al., 2015). Several studies show that OPC-encoded *HIF* function regulates cell-autonomous OPC maturation and myelination as well as WM angiogenesis via paracrine signaling (Allan et al., 2020; Yuen et al., 2014; Zhang et al., 2020). Here we extend insights into this process and show the OPCs and BVs engage in further cell-cell interactions in neonatal brain. Strikingly, we found that OPCs form what appear by ultrastructure to be direct and frequent contacts with sprouting endothelial tip cells. Our data showed tight coupling of OPC number and WM angiogenesis in transgenic mouse lines with decreased or increased OPC numbers. Together, these findings firmly establish that OPCs are major regulators of WM angiogenesis.

Embryonic OPCs depend on the vasculature for distribution throughout the CNS (Tsai et al., 2016), indicating that bi-directional cross-talk is essential during development. Moreover, during remyelination clustering of OPCs along BVs in MS lesions has been observed (Niu et al., 2019) and a recent study elucidated the role for ECs in adaptive myelination (Swire et al., 2019). Other lines of evidence indicate this relationship persists postnatally until adult stages. For example, vascular dysfunction underlies WM abnormalities in various pathological settings (Montagne et al., 2018; Rajani and Williams, 2017). Further research is warranted to investigate the complex inter-relationships between the oligodendroglial lineage and the vasculature during development and in neurological diseases.

OPC-encoded Wnt signaling is essential for neonatal white matter angiogenesis and axonal, but not BBB, integrity *in vivo*.

Angiogenesis in mouse brain is robust from E9.5 until second postnatal week (Paredes et al., 2018). Although the role of embryonic Wnt signaling and radial glia in regulation of CNS vasculature is known (Cho et al., 2017b; Cho et al., 2019; Daneman et al., 2009; Stenman et al., 2008; Zhou and Nathans, 2014), postnatal angiogenic roles for Wnt signaling in OPCs are incompletely understood. Here we incapacitated all Wnt ligand production by conditionally targeting *Wntless* with *Olig1-cre*, which drives activity in OPCs (Silbereis et al., 2014). Interestingly, while OPC number was unaffected in WM of P7 *Wntless* mutants, we found a severe impact on tip cell development and BV density, indicating that OPC-encoded Wnt activity is essential for neonatal angiogenesis. In contrast to normoxic *Olig1-cre/Wntless* mice, *Olig2-cre*, *Wnt7dKO* had a mild phenotype without impact on the developing vasculature. Because *Wntless* function is required for all Wnt ligands, and that oligodendroglia also express *Wnt 3, 4, 6, 9a* and *10a* (Zhang et al., 2014), these findings suggest that other Wnts beside *Wnt7* compensate for loss of *Wnt7a/b* during normal neonatal WM angiogenesis.

In contrast, specific roles for *Wnt7* were indicated in the setting of hypoxic injury. We found that chronic hypoxia in mouse and ferret as well as human HIE cases, showed significantly increased OPC and vessel density in WM tracts coupled with an increase in canonical Wnt/ β -catenin targets *Lef1*, *Apcdd1* and *Axin2* in ECs. In human HIE lesions, we observed *WNT7A*-expressing OPCs. Additionally, *Wnt7a/b* mutants in the hypoxic setting showed dramatic abrogation of vessel induction post-hypoxia and severe damage to WM and hypomyelination, suggesting specific roles for OPC-encoded *Wnt7* function to maintain resilience against hypoxic injury.

Canonical Wnt signaling in CNS ECs is required for BBB maturation in a region-restricted manner (Cho et al., 2017b; Wang et al., 2018; Wang et al., 2012; Zhou and Nathans, 2014; Zhou et al., 2014); for instance, loss-of-*Frizzled 4* function results in BBB disruptions only in cerebellum, retina and olfactory bulb (Wang et al., 2012). We found that neither alterations in OPC density or deletion of OPC-encoded Wnt ligand activity resulted in BBB disruption. This indicates that OPC-Wnt activity acts primarily to support endothelial tip cell development and vessel growth, but not BBB integrity.

OPC-Wnt is a primary angiogenic signal that acts in a paracrine manner in neonatal white matter.

Autocrine Wnt signaling inhibits of OPC differentiation (Fancy et al., 2009; Fancy et al., 2014; Fancy et al., 2011; Hammond et al., 2015). However, in both *Wntless* and *Wnt7dKO* mutants, we found that expression of the Wnt downstream target *Axin2* was unaltered within OPCs themselves nor did we observe precocious OPC differentiation; thus, we found no evidence for autocrine effects. Wnt ligands act as short range signals (Clevers et al., 2014) and have specific roles in brain angiogenesis (Vanhollebeke et al., 2015). We found that loss-of-OPC Wnt function in both *Wntless* and *Wnt7dKO* animals resulted in decreased WM vessel density and down-regulation of canonical Wnt/ β -catenin targets *Apcdd1* and *Axin2* in ECs, indicating cell-to-cell signaling. Moreover, OPC-Wnt signaling was specifically required to maintain expression of *Apelin* in angiogenic tip cells in contrast to other pro-angiogenic cues in *Wntless* mutants. A recent study has shown Apelin signaling promotes a pro-angiogenic state in zebrafish endothelial cells (Helker et al., 2020); loss of *Apelin* function caused tip cell defects similar mouse *Wntless* mutants described here. Because OPCs form intimate contacts with endothelial tip cells, these findings collectively indicate OPC-Wnt acts in a paracrine manner to regulate WM vascular development.

Therapeutic implications.

OPCs have been shown to react to –and be targeted in –a wide spectrum of injuries including neonatal HIE (Billiards et al., 2008; Fancy et al., 2011), stroke (Chen et al., 2018; Joseph et al., 2016) and multiple sclerosis (Fancy et al., 2011), pathologies associated with chronic hypomyelination. As angiogenesis is a fundamental initial response to a variety of tissue insults, the OPC-vascular crosstalk we describe here might also be adaptive because they can migrate rapidly along BVs into brain lesions (Niu et al., 2019). Our data suggest a new role for OPCs in this context, namely, directly regulating angiogenesis in the setting of CNS WM lesion repair. As several studies have shown abnormal OPC Wnt signaling in human neonatal white matter injury and MS (Fancy et al., 2009; Fancy et al., 2014), an implication of this study is that post-injury angiogenic wound healing could be compromised.

WM ischemic stroke is a leading cause of motor dysfunction and cognitive impairment (Roman et al., 2002), and studies in experimental models have shown that OPC numbers are upregulated during the recovery phase of the injury (Joseph et al., 2016; Sozmen et al., 2016; Zhang et al., 2011); indeed, OPC neuroprotection during the acute phase of stroke injury improves functional recovery (Chen et al., 2018). Interestingly, OPCs have been suggested to play a beneficial role in recovery by promoting post injury angiogenesis and BBB rescue in various stroke injury models (Kishida et al., 2019; Wang et al., 2020). As to the nature of

secreted pro-angiogenic cues, the current study indicates a specific function for OPC-encoded *Wnt7*.

Members of the vascular endothelial growth factor (VEGF) family are well-established hypoxic signaling targets (Himmels et al., 2017) that show developmental expression within OPCs (Cahoy et al., 2008). Indeed, VEGF expression has also been reported to be regulated by canonical Wnt signaling (Easwaran et al., 2003; Wu et al., 2015). Similarly, other pro-angiogenic candidate factors such as semaphorins and neuropilins are also expressed by oligodendroglial lineage cells. Because, aged patients show diminished recovery from stroke compared to young adults (Boussier, 2012; Ovbiagele and Nguyen-Huynh, 2011), and OPC functions decline in aged animals (Ruckh et al., 2012), a related question is how OPC angiogenic factor production is regulated over the life course? Future work is needed to investigate OPC-encoded regulators of BV development over the life course and their functional relevance in neonatal, juvenile and/or adult WM injuries.

STAR METHODS

RESOURCE AVAILABILITY

Lead Contact—Further information and requests for resources and reagents should be directed to and will be fulfilled by the Lead Contact, David H Rowitch (dhr25@medschl.cam.ac.uk).

Materials Availability—All unique reagents/materials generated in this study will be available from the Lead contact upon completion of pertinent material transfer agreement.

Data and Code Availability—This study did not generate any code.

EXPERIMENTAL MODEL AND SUBJECT DETAILS

All animal procedures were performed according to the University of California at San Francisco guidelines under Institutional Animal Care and Use Program (IACUC) approved protocols. Age of the mice/ferrets used for the study are identified in the main text and figure legends. Animals were housed under standard 12-hour light/dark cycle conditions and were fed ad libitum. The following mouse lines were used in the study: *Olig2-cre* mouse line was previously described (Schuller et al., 2008). Briefly, the line was generated by inserting an avian-specific retroviral receptor, and an IRES-cre recombinase cassette into the endogenous *Olig2* locus by homologous recombination. *Sox10-DTA* mice have been generated by Dr. William Richardson's lab and are previously described (Kessaris et al., 2006). *BRAF^{CA}* is a knock-in allele of human BRAf which expresses normal BRAf prior to Cre recombinase exposure and encodes mutationally activated BRAF^{V600E} after Cre recombination (Dankort et al., 2009). *Olig1Cre* mouse line was generated by inserting a cre-neo cassette into the *Olig1* locus via homologous recombination and was previously described (Lu et al., 2002). *Wis floxed (Wntless)* mice were purchased from Jackson laboratory and are previously described (Carpenter et al., 2010). *Wnt7dKO* mice were generated by intercrossing *Olig2-Cre* mouse line to *Wnt7a^{+/-}* and *Wnt7b (fl/fl)* lines (Stenman et al., 2008). Note that *Wnt7a^{-/-}* mice are infertile so they were bred as heterozygotes. For experiments involving

transgenic animals, littermates were randomly assigned to experimental groups with approximately equal amounts of male and female animals.

Chronic hypoxic rearing was performed as previously described (Yuen et al., 2014). Briefly, litters from Control or *Wnt7dKO* animals were culled to a size of 4 pups and co-fostered with lactating CD1 strain dams then reared at 10% O₂ in a hypoxic chamber starting on postnatal day 3 (P3) (Biospherix, Inc., Laconia, NY). Dams were provided ad libitum access to water and food. Mice were monitored daily to ensure that there are no signs of distress, poor intake of food and water, unusual/decreased grooming. Tissue from P11 pups were then harvested for analysis within 1 hour after removal from hypoxia chamber.

To perform ferret chronic sublethal hypoxia experiments, pregnant jills were obtained from Marshall Farms (North Rose, NY) at E26 gestation. The kits from these ferrets along with the jill were placed in a 10% oxygen chamber on postnatal day 10 (P10) until P20 endpoint. The health of kits and jill were monitored daily (lethargy, poor weight gain and failure to nurse). Animals were provided ad libitum access to water and food and supplemented as required. On P20 kits were euthanized within 1 hour after removal from their housing by deeply anesthetizing with isoflurane in an anesthesia chamber. After loss of righting reflex, the animals were transcardially perfused with PBS followed by 4% PFA. Following perfusion, brains were removed from the skull using forceps or a bone rongeur.

Human Neonatal Brain Specimen—This study involves use of de-identified human post-mortem fixed-frozen brain tissue samples obtained from University of California, San Francisco's Pediatric Neuropathology Research Laboratory (see Table S1 for clinicopathological information). Tissue was fixed with 4% paraformaldehyde, followed by sequential immersion in 10%, 20% and 30% sucrose for cryopreservation. Frozen tissues are sectioned at 14 μm for immunohistochemistry and smFISH applications. All the HIE cases in this study showed evidence of diffuse white matter injury, with astrogliosis and macrophage infiltration (Figure S5). It must be noted that although some control brain specimens were obtained from diaphragmatic hernia cases, which may result in hypoxemia, these specimens were examined and classified as “control” by an experienced neuropathologist and did not exhibit any evidence of astrogliosis or macrophage infiltration. Both male and female cases from control and HIE conditions were analyzed, and we did not observe any gender association on the results reported.

METHOD DETAILS

Tissue Processing and Immunohistochemistry—Mice were deeply anesthetized and transcardially perfused with cold PBS followed by cold 4% PFA. Brains were isolated and post-fixed overnight in 4% PFA and cryoprotected in 30% sucrose for 24 hours and then frozen at –80°C until sectioned. Frozen brains were sectioned at 30μm thickness. Tissue sections were blocked for 1 hour using blocking solution (5% horse serum/0.3% Triton X-100 in PBS) and incubated with primary antibodies (resource table) overnight at 4°C in fresh blocking solution. Sections were washed thrice in PBS containing 0.4% Triton X-100 followed by incubation with the appropriate secondary antibodies purchased from Invitrogen. Three to five additional washes were performed, and sections were mounted

using DAPI-Fluoromount G (SouthernBiotech). Antigen retrieval was performed by pre-treating the sections for 10 minutes at 95°C in 10mM Sodium Citrate (pH 6.0) in a microwave oven (BioWave). Histological preparations were analyzed using Leica Sp5 upright AOBS confocal microscope. Images were acquired with either 20x, 40x or 63x objectives.

Olig2 Immunogold Labeling and Electron Microscopy Processing—The specimen was obtained by a surgical resection of the right temporal lobe from a 2year old female with type IIB focal cortical dysplasia. The tissue was fixed in 4% PFA in 0.1M PBS for 7 days. After 100 µm sections were obtained using a Leica VT1000S vibratome (Leica Biosystems, Wetzlar, Germany). For pre-embedding immunogold, the tissue was cryoprotected in a solution containing 25% saccharose in 0.1M phosphate buffer (PB) for 30 min followed by repeated freeze-thaw cycles for permeabilization. The permeabilization step was performed by immersing the samples repeatedly in –60°C 2-methylbutane and transferring them to room temperature saccharose solution. After, the samples were incubated in a blocking solution consisting of 0.3% BSAc (Aurion, Wageningen, the Netherlands), 0.05% sodium azide in 0.1 M PB for 1 h. Subsequently, the samples were incubated in primary antibody (1:150 rabbit anti-Olig2, Millipore) in blocking solution for 72 h at 4°C. The sections were then rinsed in 0.1 M PB and incubated in secondary antibody blocking solution consisting of 0.5% BSAc (Aurion), 0.025% CWFS gelatin (Aurion), 0.05% sodium azide in 0.1 M PB for 1 h, followed by incubation in secondary antibody (1:50 goat-anti-rabbit IgG gold ultrasmall; Aurion) diluted in the same solution overnight at 4°C. To enhance gold labeling, we performed silver enhancement (R-GENT SE-LM, Aurion) for 15–25 min in the dark, followed by gentle washing in 2% sodium acetate and incubation in gold toning solution (0.05% gold chloride in water) for 10 min. The sections were then washed twice with 0.3% sodium thiosulfate in water. Finally, we post fixed with 2% glutaraldehyde (Electron Microscopy Sciences) in 0.1M PB for 30 min.

For transmission electron microscopy analysis, specimen was post fixed with 1% osmium tetroxide (Electron Microscopy Sciences), 7% glucose in 0.1M PB for 30 min at room temperature, washed in deionized water, and partially dehydrated in 70% ethanol. Afterwards, the samples were contrasted in 2% uranyl acetate (Electron Microscopy Sciences) in 70% ethanol for 2 hours at 4°C. The samples were further dehydrated and embedded in Durcupan ACM epoxy resin (Sigma-Aldrich) at room temperature overnight, and then at 60°C for 72 h. Once the resin was polymerized, immunolabeled sections were selected and cut into semithin (1.5 µm) and ultrathin (60–80 nm) sections using a UC6 ultramicrotome (Leica Biosystems). These sections were placed on Formvar-coated single-slot copper grids (Electron Microscopy Sciences) stained with lead citrate and examined at 80 kV on a FEI Tecnai G2 Spirit (FEI Company, Hillsboro, OR) transmission electron microscope equipped with a Morada CCD digital camera (Olympus, Tokyo, Japan).

Single molecule fluorescent *in situ* hybridization—Three-color smFISH was performed on fixed frozen sections from human neonatal brain specimen or control and mutant mice using Advanced Cell Diagnostics RNAscope® Fluorescent Multiplex Reagent Kit and probes. Cryosections (14µm thick) were mounted on glass slides and washed in

presented as average number of branches per unit area quantified. Total vascular length was quantified as the sum of lengths of all vessels in a field.

Microscopy and Cell Counting—Optical sections of confocal epifluorescence images were sequentially acquired using LAS AF software (Leica). Images were merged using ImageJ software and merged images were processed on Adobe Illustrator software. Background modifications, where required for presentation purposes, were applied evenly across the entire image and between the control and experimental groups using Leica's LAS software or ImageJ. At least $n=4-7$ different animals for each experimental condition were collected and analyzed as indicated in the respective figure legends. Matched sections between -2.5 and $+1.10$ bregma were used for analysis and the regions indicated in figures were analyzed. Typically, 3–6 fields from 6–8 non-adjacent sections were analyzed per animal and counts are presented as the number of cells per 1 mm^2 or percentage of cells within the indicated cell population. All counts were performed using ImageJ software. All cell counts were performed with the researcher blinded to condition.

QUANTIFICATION AND STATISTICAL ANALYSIS

Data are represented as mean \pm S.D. and the number of experiments, cases analyzed and animals per genotype and condition are indicated in all figure legends. No statistical methods were used to predetermine the sample size. No data were excluded from analyses. Statistical analysis was performed using the two tailed unpaired Student's ttest. A "p" value < 0.05 was considered significant. In all cases, * indicates a p value < 0.05 , ** < 0.01 , and *** $p < 0.001$, **** $p < 0.0001$. All the data analysis and plotting were performed on GraphPad Prism version 6.0.

Supplementary Material

Refer to Web version on PubMed Central for supplementary material.

ACKNOWLEDGEMENTS

We would like to thank members of the Rowitch lab for their valuable suggestions and technical assistance with experimental setup. J.M.G.V and M.J.U.N would like to acknowledge Patricia García-Tárraga and Ana Sauri-Tamarit for their assistance with electron microscopy experiments. We would also like to thank Sasha Mikhailova for assistance with ferret hypoxia experiments. M.C. acknowledges fellowship awards from the American Heart Association and The Children's Heart Foundation and funding support from a Career Development Grant awarded by Cerebral Palsy Alliance Research Foundation. J.M.G.V is funded by Red deTerapia Celular (TerCel-RD16/0011/0026) and the Valencian Council for Innovation, Universities Science and Digital Society (PROMETEO/2019/075). M.J.U.N was supported by a McDonald Fellowship from the Multiple Sclerosis International Federation. This work was supported by funding from the National Multiple Sclerosis Foundation (to D.H.R.), the Adelson Medical Research Foundation (D.H.R.), the European Research Council (D.H.R.) and the National Institutes of Health, NINDS (1K99NS117804 to M.C; P01NS083513 to D.H.R., E.J.H and P.S.M).

REFERENCES

- Adams RH, and Eichmann A (2010). Axon guidance molecules in vascular patterning. *Cold Spring Harb Perspect Biol* 2, a001875. [PubMed: 20452960]
- Allan KC, Hu LR, Morton AR, Scavuzzo MA, Gevorgyan AS, Clayton BLL, Bederman IR, Hung S, Bartels CF, Madhavan M, et al. (2020). Non-Canonical Targets of HIF1 α Drive Cell-Type-Specific Dysfunction. *bioRxiv*, 2020.2004.2003.003632.

- Arnett HA, Fancy SP, Alberta JA, Zhao C, Plant SR, Kaing S, Raine CS, Rowitch DH, Franklin RJ, and Stiles CD (2004). bHLH transcription factor *Olig1* is required to repair demyelinated lesions in the CNS. *Science* 306, 2111–2115. [PubMed: 15604411]
- Banziger C, Soldini D, Schutt C, Zipperlen P, Hausmann G, and Basler K (2006). Wntless, a conserved membrane protein dedicated to the secretion of Wnt proteins from signaling cells. *Cell* 125, 509–522. [PubMed: 16678095]
- Baron W, and Hoekstra D (2010). On the biogenesis of myelin membranes: sorting, trafficking and cell polarity. *FEBS Lett* 584, 1760–1770. [PubMed: 19896485]
- Billiards SS, Haynes RL, Folkerth RD, Borenstein NS, Trachtenberg FL, Rowitch DH, Ligon KL, Volpe JJ, and Kinney HC (2008). Myelin abnormalities without oligodendrocyte loss in periventricular leukomalacia. *Brain Pathol* 18, 153–163. [PubMed: 18177464]
- Boussier MG (2012). Stroke prevention: an update. *Front Med* 6, 22–34. [PubMed: 22460445]
- Bozoyan L, Khlghatyan J, and Saghatelian A (2012). Astrocytes control the development of the migration-promoting vasculature scaffold in the postnatal brain via VEGF signaling. *J Neurosci* 32, 1687–1704. [PubMed: 22302810]
- Cahoy JD, Emery B, Kaushal A, Foo LC, Zamanian JL, Christopherson KS, Xing Y, Lubischer JL, Krieg PA, Krupenko SA, et al. (2008). A transcriptome database for astrocytes, neurons, and oligodendrocytes: a new resource for understanding brain development and function. *J Neurosci* 28, 264–278. [PubMed: 18171944]
- Carmeliet P, and Jain RK (2011). Molecular mechanisms and clinical applications of angiogenesis. *Nature* 473, 298–307. [PubMed: 21593862]
- Carpenter AC, Rao S, Wells JM, Campbell K, and Lang RA (2010). Generation of mice with a conditional null allele for Wntless. *Genesis* 48, 554–558. [PubMed: 20614471]
- Chen Y, Zhang L, Yu H, Song K, Shi J, Chen L, and Cheng J (2018). Necrostatin-1 Improves Long-term Functional Recovery Through Protecting Oligodendrocyte Precursor Cells After Transient Focal Cerebral Ischemia in Mice. *Neuroscience* 371, 229–241. [PubMed: 29247776]
- Cho C, Smallwood PM, and Nathans J (2017a). Reck and Gpr124 Are Essential Receptor Cofactors for Wnt7a/Wnt7b-Specific Signaling in Mammalian CNS Angiogenesis and Blood-Brain Barrier Regulation. *Neuron* 95, 1221–1225.
- Cho C, Smallwood PM, and Nathans J (2017b). Reck and Gpr124 Are Essential Receptor Cofactors for Wnt7a/Wnt7b-Specific Signaling in Mammalian CNS Angiogenesis and Blood-Brain Barrier Regulation. *Neuron* 95, 1056–1073 e1055. [PubMed: 28803732]
- Cho C, Wang Y, Smallwood PM, Williams J, and Nathans J (2019). Molecular determinants in Frizzled, Reck, and Wnt7a for ligand-specific signaling in neurovascular development. *Elife* 8.
- Clevers H, Loh KM, and Nusse R (2014). Stem cell signaling. An integral program for tissue renewal and regeneration: Wnt signaling and stem cell control. *Science* 346, 1248012. [PubMed: 25278615]
- Daneman R, Agalliu D, Zhou L, Kuhnert F, Kuo CJ, and Barres BA (2009). Wnt/beta-catenin signaling is required for CNS, but not non-CNS, angiogenesis. *Proc Natl Acad Sci U S A* 106, 641–646. [PubMed: 19129494]
- Dankort D, Curley DP, Cartledge RA, Nelson B, Karnezis AN, Damsky WE Jr., You MJ, DePinho RA, McMahon M, and Bosenberg M (2009). Braf(V600E) cooperates with Pten loss to induce metastatic melanoma. *Nat Genet* 41, 544–552. [PubMed: 19282848]
- del Toro R, Prahst C, Mathivet T, Siegfried G, Kaminker JS, Larrivee B, Breant C, Duarte A, Takakura N, Fukamizu A, et al. (2010). Identification and functional analysis of endothelial tip cell-enriched genes. *Blood* 116, 4025–4033. [PubMed: 20705756]
- Easwaran V, Lee SH, Inge L, Guo L, Goldbeck C, Garrett E, Wiesmann M, Garcia PD, Fuller JH, Chan V, et al. (2003). beta-Catenin regulates vascular endothelial growth factor expression in colon cancer. *Cancer Res* 63, 3145–3153. [PubMed: 12810642]
- Eichmann A, and Thomas JL (2013). Molecular parallels between neural and vascular development. *Cold Spring Harb Perspect Med* 3, a006551. [PubMed: 23024177]
- Fancy SP, Baranzini SE, Zhao C, Yuk DI, Irvine KA, Kaing S, Sanai N, Franklin RJ, and Rowitch DH (2009). Dysregulation of the Wnt pathway inhibits timely myelination and remyelination in the mammalian CNS. *Genes Dev* 23, 1571–1585. [PubMed: 19515974]

- Fancy SP, Harrington EP, Baranzini SE, Silbereis JC, Shiow LR, Yuen TJ, Huang EJ, Lomvardas S, and Rowitch DH (2014). Parallel states of pathological Wnt signaling in neonatal brain injury and colon cancer. *Nat Neurosci* 17, 506–512. [PubMed: 24609463]
- Fancy SP, Harrington EP, Yuen TJ, Silbereis JC, Zhao C, Baranzini SE, Bruce CC, Otero JJ, Huang EJ, Nusse R, et al. (2011). Axin2 as regulatory and therapeutic target in newborn brain injury and remyelination. *Nat Neurosci* 14, 1009–1016. [PubMed: 21706018]
- Fantini A, Lampropoulou A, Gestri G, Raimondi C, Senatore V, Zachary I, and Ruhrberg C (2015). NRP1 Regulates CDC42 Activation to Promote Filopodia Formation in Endothelial Tip Cells. *Cell Rep* 11, 1577–1590. [PubMed: 26051942]
- Fard MK, van der Meer F, Sanchez P, Cantuti-Castelvetri L, Mandad S, Jakel S, Fornasiero EF, Schmitt S, Ehrlich M, Starost L, et al. (2017). BCAS1 expression defines a population of early myelinating oligodendrocytes in multiple sclerosis lesions. *Sci Transl Med* 9.
- Greenberg DA, and Jin K (2005). From angiogenesis to neuropathology. *Nature* 438, 954–959. [PubMed: 16355213]
- Grutzendler J, Murkinati S, Hiner B, Ji L, Lam CK, Yoo T, Gupta S, Hafner BP, Adelman RA, Yuan P, et al. (2014). Angiophagy prevents early embolus washout but recanalizes microvessels through embolus extravasation. *Sci Transl Med* 6, 226ra231.
- Hammond E, Lang J, Maeda Y, Pleasure D, Angus-Hill M, Xu J, Horiuchi M, Deng W, and Guo F (2015). The Wnt effector transcription factor 7-like 2 positively regulates oligodendrocyte differentiation in a manner independent of Wnt/beta-catenin signaling. *J Neurosci* 35, 5007–5022. [PubMed: 25810530]
- Harb R, Whiteus C, Freitas C, and Grutzendler J (2013). In vivo imaging of cerebral microvascular plasticity from birth to death. *J Cereb Blood Flow Metab* 33, 146–156. [PubMed: 23093067]
- Harris JJ, and Attwell D (2012). The energetics of CNS white matter. *J Neurosci* 32, 356–371. [PubMed: 22219296]
- Helker CS, Eberlein J, Wilhelm K, Sugino T, Malchow J, Schuermann A, Baumeister S, Kwon HB, Maischein HM, Potente M, et al. (2020). Apelin signaling drives vascular endothelial cells towards a pro-angiogenic state. *Elife* 9.
- Himmels P, Paredes I, Adler H, Karakatsani A, Luck R, Marti HH, Ermakova O, Rempel E, Stoeckli ET, and Ruiz de Almodovar C (2017). Motor neurons control blood vessel patterning in the developing spinal cord. *Nat Commun* 8, 14583. [PubMed: 28262664]
- Huillard E, Hashizume R, Phillips JJ, Griveau A, Ihrie RA, Aoki Y, Nicolaidis T, Perry A, Waldman T, McMahon M, et al. (2012). Cooperative interactions of BRAFV600E kinase and CDKN2A locus deficiency in pediatric malignant astrocytoma as a basis for rational therapy. *Proc Natl Acad Sci U S A* 109, 8710–8715. [PubMed: 22586120]
- Joseph MJ, Caliaperumal J, and Schlichter LC (2016). After Intracerebral Hemorrhage, Oligodendrocyte Precursors Proliferate and Differentiate Inside White-Matter Tracts in the Rat Striatum. *Transl Stroke Res* 7, 192–208. [PubMed: 26743212]
- Kessaris N, Fogarty M, Iannarelli P, Grist M, Wegner M, and Richardson WD (2006). Competing waves of oligodendrocytes in the forebrain and postnatal elimination of an embryonic lineage. *Nat Neurosci* 9, 173–179. [PubMed: 16388308]
- Kidoya H, and Takakura N (2012). Biology of the apelin-APJ axis in vascular formation. *J Biochem* 152, 125–131. [PubMed: 22745157]
- Kinney HC, and Back SA (1998). Human oligodendroglial development: relationship to periventricular leukomalacia. *Semin Pediatr Neurol* 5, 180–189. [PubMed: 9777676]
- Kishida N, Maki T, Takagi Y, Yasuda K, Kinoshita H, Ayaki T, Noro T, Kinoshita Y, Ono Y, Kataoka H, et al. (2019). Role of Perivascular Oligodendrocyte Precursor Cells in Angiogenesis After Brain Ischemia. *J Am Heart Assoc* 8, e011824. [PubMed: 31020902]
- Lam CK, Yoo T, Hiner B, Liu Z, and Grutzendler J (2010). Embolus extravasation is an alternative mechanism for cerebral microvascular recanalization. *Nature* 465, 478–482. [PubMed: 20505729]
- Le Magueresse C, Alfonso J, Bark C, Eliava M, Khrulev S, and Monyer H (2012). Subventricular zone-derived neuroblasts use vasculature as a scaffold to migrate radially to the cortex in neonatal mice. *Cereb Cortex* 22, 2285–2296. [PubMed: 22095212]

- Liu F, and McCullough LD (2013). Inflammatory responses in hypoxic ischemic encephalopathy. *Acta Pharmacol Sin* 34, 1121–1130. [PubMed: 23892271]
- Lord SJ, Velle KB, Mullins RD, and Fritz-Laylin LK (2020). SuperPlots: Communicating reproducibility and variability in cell biology. *J Cell Biol* 219.
- Lu QR, Sun T, Zhu Z, Ma N, Garcia M, Stiles CD, and Rowitch DH (2002). Common developmental requirement for Olig function indicates a motor neuron/oligodendrocyte connection. *Cell* 109, 75–86. [PubMed: 11955448]
- Ma S, Kwon HJ, Johng H, Zang K, and Huang Z (2013). Radial glial neural progenitors regulate nascent brain vascular network stabilization via inhibition of Wnt signaling. *PLoS Biol* 11, e1001469. [PubMed: 23349620]
- Minocha S, Valloton D, Brunet I, Eichmann A, Hornung JP, and Lebrand C (2015). NG2 glia are required for vessel network formation during embryonic development. *Elife* 4.
- Montagne A, Nikolakopoulou AM, Zhao Z, Sagare AP, Si G, Lazic D, Barnes SR, Daianu M, Ramanathan A, Go A, et al. (2018). Pericyte degeneration causes white matter dysfunction in the mouse central nervous system. *Nat Med* 24, 326–337. [PubMed: 29400711]
- Niu J, Tsai HH, Hoi KK, Huang N, Yu G, Kim K, Baranzini SE, Xiao L, Chan JR, and Fancy SPJ (2019). Aberrant oligodendroglial-vascular interactions disrupt the blood-brain barrier, triggering CNS inflammation. *Nat Neurosci* 22, 709–718. [PubMed: 30988524]
- Northington FJ, Chavez-Valdez R, and Martin LJ (2011). Neuronal cell death in neonatal hypoxia-ischemia. *Ann Neurol* 69, 743–758. [PubMed: 21520238]
- Ovbiagele B, and Nguyen-Huynh MN (2011). Stroke epidemiology: advancing our understanding of disease mechanism and therapy. *Neurotherapeutics* 8, 319–329. [PubMed: 21691873]
- Paredes I, Himmels P, and Ruiz de Almodovar C (2018). Neurovascular Communication during CNS Development. *Dev Cell* 45, 10–32. [PubMed: 29634931]
- Plate KH (1999). Mechanisms of angiogenesis in the brain. *J Neuropathol Exp Neurol* 58, 313320.
- Rajani RM, Quick S, Ruigrok SR, Graham D, Harris SE, Verhaaren BFJ, Fornage M, Seshadri S, Atanur SS, Dominiczak AF, et al. (2018). Reversal of endothelial dysfunction reduces white matter vulnerability in cerebral small vessel disease in rats. *Sci Transl Med* 10.
- Rajani RM, and Williams A (2017). Endothelial cell-oligodendrocyte interactions in small vessel disease and aging. *Clin Sci (Lond)* 131, 369–379. [PubMed: 28202749]
- Roman GC, Erkinjuntti T, Wallin A, Pantoni L, and Chui HC (2002). Subcortical ischaemic vascular dementia. *Lancet Neurol* 1, 426–436. [PubMed: 12849365]
- Ruckh JM, Zhao JW, Shadrach JL, van Wijngaarden P, Rao TN, Wagers AJ, and Franklin RJ (2012). Rejuvenation of regeneration in the aging central nervous system. *Cell Stem Cell* 10, 96–103. [PubMed: 22226359]
- Schuller U, Heine VM, Mao J, Kho AT, Dillon AK, Han YG, Huillard E, Sun T, Ligon AH, Qian Y, et al. (2008). Acquisition of granule neuron precursor identity is a critical determinant of progenitor cell competence to form Shh-induced medulloblastoma. *Cancer Cell* 14, 123–134. [PubMed: 18691547]
- Segarra M, Aburto MR, Cop F, Llao-Cid C, Hartl R, Damm M, Bethani I, Parrilla M, Husainie D, Schanzer A, et al. (2018). Endothelial Dab1 signaling orchestrates neuro-gliavessel communication in the central nervous system. *Science* 361.
- Shen J, Wang D, Wang X, Gupta S, Ayloo B, Wu S, Prasad P, Xiong Q, Xia J, and Ge S (2019). Neurovascular Coupling in the Dentate Gyrus Regulates Adult Hippocampal Neurogenesis. *Neuron* 103, 878–890 e873. [PubMed: 31257104]
- Silbereis JC, Nobuta H, Tsai HH, Heine VM, McKinsey GL, Meijer DH, Howard MA, Petryniak MA, Potter GB, Alberta JA, et al. (2014). Olig1 function is required to repress dlx1/2 and interneuron production in Mammalian brain. *Neuron* 81, 574–587. [PubMed: 24507192]
- Sozmen EG, Rosenzweig S, Llorente IL, DiTullio DJ, Machnicki M, Vinters HV, Havton LA, Giger RJ, Hinman JD, and Carmichael ST (2016). Nogo receptor blockade overcomes remyelination failure after white matter stroke and stimulates functional recovery in aged mice. *Proc Natl Acad Sci U S A* 113, E8453–E8462. [PubMed: 27956620]

- Stenman JM, Rajagopal J, Carroll TJ, Ishibashi M, McMahon J, and McMahon AP (2008). Canonical Wnt signaling regulates organ-specific assembly and differentiation of CNS vasculature. *Science* 322, 1247–1250. [PubMed: 19023080]
- Swire M, Kotelevtsev Y, Webb DJ, Lyons DA, and French-Constant C (2019). Endothelin signalling mediates experience-dependent myelination in the CNS. *Elife* 8.
- Tao JD, Barnette AR, Griffith JL, Neil JJ, and Inder TE (2012). Histopathologic correlation with diffusion tensor imaging after chronic hypoxia in the immature ferret. *Pediatr Res* 71, 192–198. [PubMed: 22258131]
- Tavazoie M, Van der Veken L, Silva-Vargas V, Louissaint M, Colonna L, Zaidi B, Garcia-Verdugo JM, and Doetsch F (2008). A specialized vascular niche for adult neural stem cells. *Cell Stem Cell* 3, 279–288. [PubMed: 18786415]
- Tsai HH, Niu J, Munji R, Davalos D, Chang J, Zhang H, Tien AC, Kuo CJ, Chan JR, Daneman R, et al. (2016). Oligodendrocyte precursors migrate along vasculature in the developing nervous system. *Science* 351, 379–384. [PubMed: 26798014]
- Vanhollebeke B, Stone OA, Bostaille N, Cho C, Zhou Y, Maquet E, Gauquier A, Cabochette P, Fukuhara S, Mochizuki N, et al. (2015). Tip cell-specific requirement for an atypical Gpr124- and Reck-dependent Wnt/beta-catenin pathway during brain angiogenesis. *Elife* 4.
- Vasudevan A, Long JE, Crandall JE, Rubenstein JL, and Bhide PG (2008). Compartment-specific transcription factors orchestrate angiogenesis gradients in the embryonic brain. *Nat Neurosci* 11, 429–439. [PubMed: 18344991]
- Wang J, Cui Y, Yu Z, Wang W, Cheng X, Ji W, Guo S, Zhou Q, Wu N, Chen Y, et al. (2019). Brain Endothelial Cells Maintain Lactate Homeostasis and Control Adult Hippocampal Neurogenesis. *Cell Stem Cell* 25, 754–767 e759. [PubMed: 31761722]
- Wang L, Geng J, Qu M, Yuan F, Wang Y, Pan J, Li Y, Ma Y, Zhou P, Zhang Z, et al. (2020). Oligodendrocyte precursor cells transplantation protects blood-brain barrier in a mouse model of brain ischemia via Wnt/beta-catenin signaling. *Cell Death Dis* 11, 9. [PubMed: 31907363]
- Wang Y, Cho C, Williams J, Smallwood PM, Zhang C, Junge HJ, and Nathans J (2018). Interplay of the Norrin and Wnt7a/Wnt7b signaling systems in blood-brain barrier and bloodretina barrier development and maintenance. *Proc Natl Acad Sci U S A* 115, E11827–E11836. [PubMed: 30478038]
- Wang Y, Rattner A, Zhou Y, Williams J, Smallwood PM, and Nathans J (2012). Norrin/Frizzled4 signaling in retinal vascular development and blood brain barrier plasticity. *Cell* 151, 1332–1344. [PubMed: 23217714]
- Webster HD (1971). The geometry of peripheral myelin sheaths during their formation and growth in rat sciatic nerves. *J Cell Biol* 48, 348–367. [PubMed: 4928020]
- Wu C, Chen J, Chen C, Wang W, Wen L, Gao K, Chen X, Xiong S, Zhao H, and Li S (2015). Wnt/beta-catenin coupled with HIF-1alpha/VEGF signaling pathways involved in galangin neurovascular unit protection from focal cerebral ischemia. *Sci Rep* 5, 16151. [PubMed: 26537366]
- Yuen TJ, Silbereis JC, Griveau A, Chang SM, Daneman R, Fancy SPJ, Zahed H, Maltepe E, and Rowitch DH (2014). Oligodendrocyte-encoded HIF function couples postnatal myelination and white matter angiogenesis. *Cell* 158, 383–396. [PubMed: 25018103]
- Zhang RL, Chopp M, Roberts C, Jia L, Wei M, Lu M, Wang X, Pourabdollah S, and Zhang ZG (2011). Ascl1 lineage cells contribute to ischemia-induced neurogenesis and oligodendrogenesis. *J Cereb Blood Flow Metab* 31, 614–625. [PubMed: 20736965]
- Zhang S, Kim B, Zhu X, Gui X, Wang Y, Lan Z, Prabhu P, Fond K, Wang A, and Guo F (2020). Glial type specific regulation of CNS angiogenesis by HIF1alpha-activated different signaling pathways. *Nat Commun* 11, 2027. [PubMed: 32332719]
- Zhang Y, Chen K, Sloan SA, Bennett ML, Scholze AR, O’Keeffe S, Phatnani HP, Guarnieri P, Caneda C, Ruderisch N, et al. (2014). An RNA-sequencing transcriptome and splicing database of glia, neurons, and vascular cells of the cerebral cortex. *J Neurosci* 34, 11929–11947. [PubMed: 25186741]
- Zhou Y, and Nathans J (2014). Gpr124 controls CNS angiogenesis and blood-brain barrier integrity by promoting ligand-specific canonical wnt signaling. *Dev Cell* 31, 248–256. [PubMed: 25373781]

Zhou Y, Wang Y, Tischfield M, Williams J, Smallwood PM, Rattner A, Taketo MM, and Nathans J (2014). Canonical WNT signaling components in vascular development and barrier formation. *J Clin Invest* 124, 3825–3846. [PubMed: 25083995]

Author Manuscript

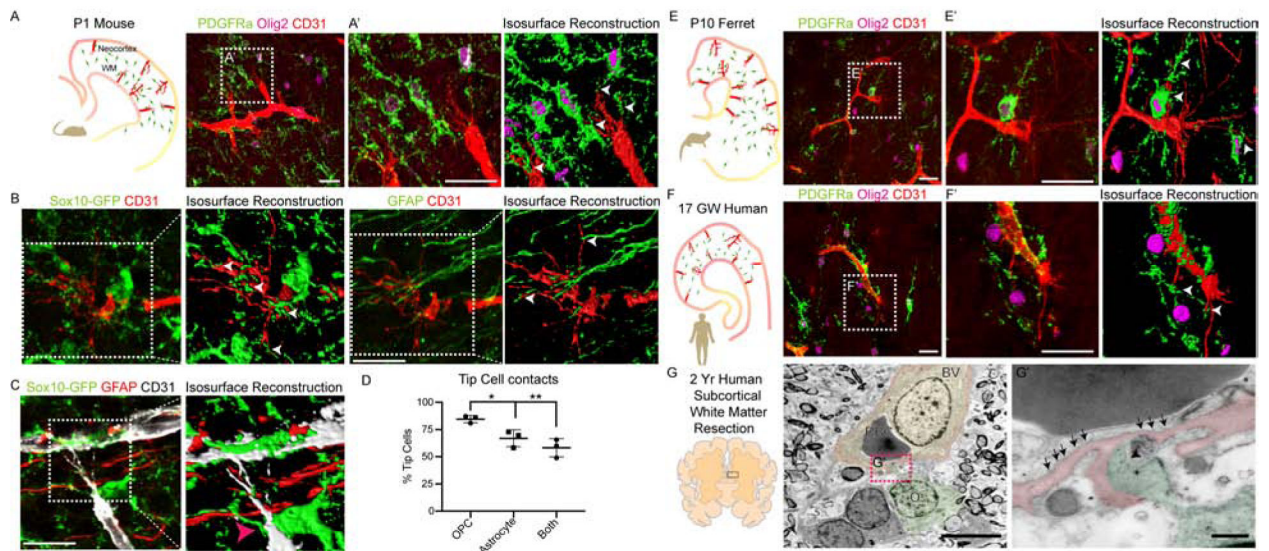
Author Manuscript

Author Manuscript

Author Manuscript

Highlights

- OPC density promotes white matter vascularization through tip cell angiogenesis.
- Hypoxic OPCs in human HIE lesions activate canonical Wnt pathway in endothelium.
- OPC-Wntless cKO caused disrupted tip cell angiogenesis and myelination deficits.
- OPC-Wnt7a/7b double KO mice display increased susceptibility to hypoxic injury.



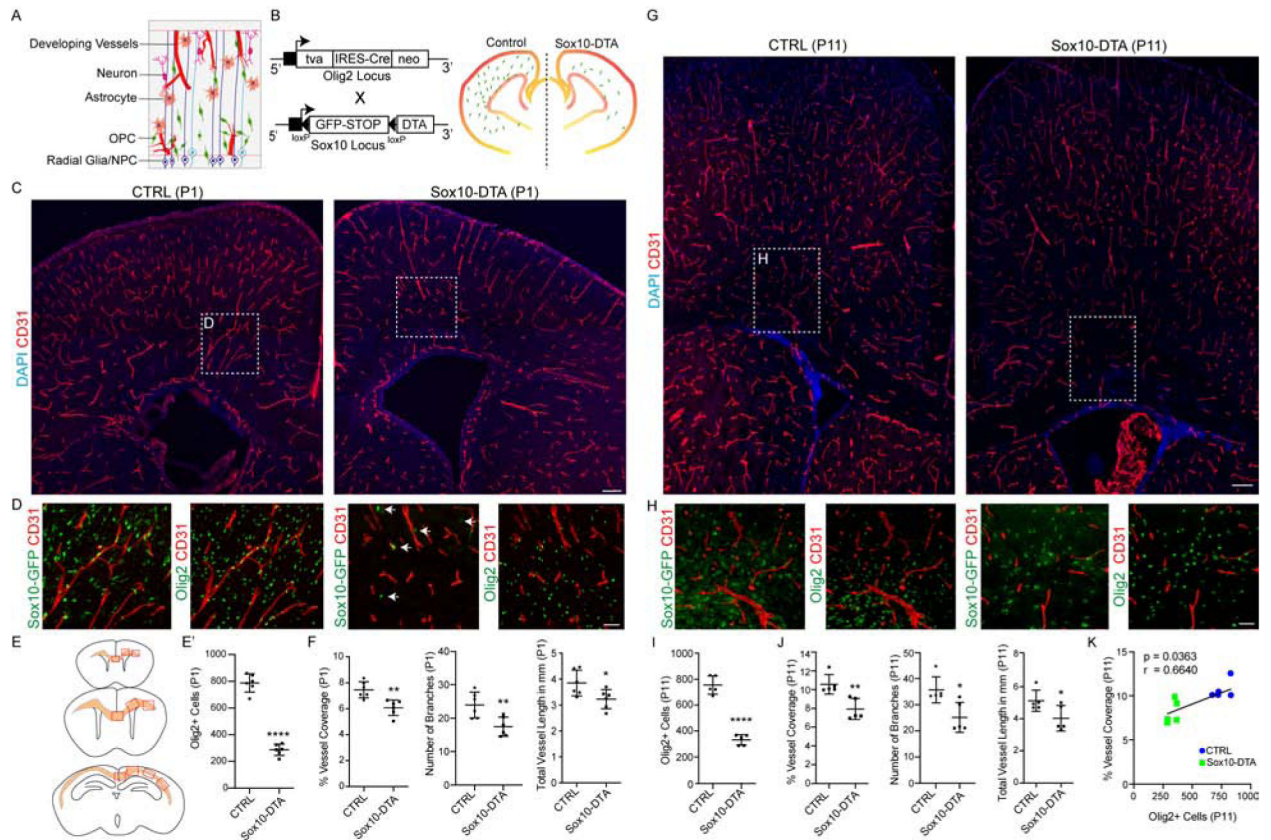


Figure 2: OPC Ablation Leads to Developmental Hypovascularization of White Matter in *Sox10-DTA* Transgenic Mice

(A) Cartoon of neuronal and glial interactions with developing vasculature in the postnatal forebrain.

(B) Genetic strategy for *Sox10-DTA* transgenic mouse generation.

(C) Representative images of P1 - Control (CTRL) and *Sox10-DTA* mouse coronal brain sections labelled with CD31 showing significant decrease in WM vessel density. Scale bar = 100 μ m

(D) High magnification images of cingulum region (from (C)), showing Sox10-GFP+Olig2+ oligodendroglial cells and CD31+ BVs. Scale bar = 50 μ m

(E) Regions of WM analyzed along the rostro-caudal axis.

(E') Quantification of Olig2+ cells in the P1 WM.

(F) Quantification of P1 BV coverage, branching and length in WM.

(g) Coronal sections from P11- Control (CTRL) and *Sox10-DTA* mouse brains labelled with CD31 showing significant decrease in WM vessel density. Scale bar = 100 μ m

(H) High magnification images of cingulum region (highlighted areas from (G)), showing Sox10-GFP+Olig2+ oligodendroglial cells and CD31+ BVs. Scale bar = 50 μ m.

(I) Quantification of Olig2+ cells in the P11 WM.

(J) Quantification of P11 BV coverage, branching and length in WM.

(K) Oligodendroglial cell density and vessel coverage in WM are positively correlated. Data are represented as mean \pm S.D. and analyzed by two-tailed unpaired Student's t test. $n=6$ animals/genotype (E'–F); $n=5$ (I–K). Significance: * $p<0.05$, ** $p<0.01$, **** $p<0.0001$.

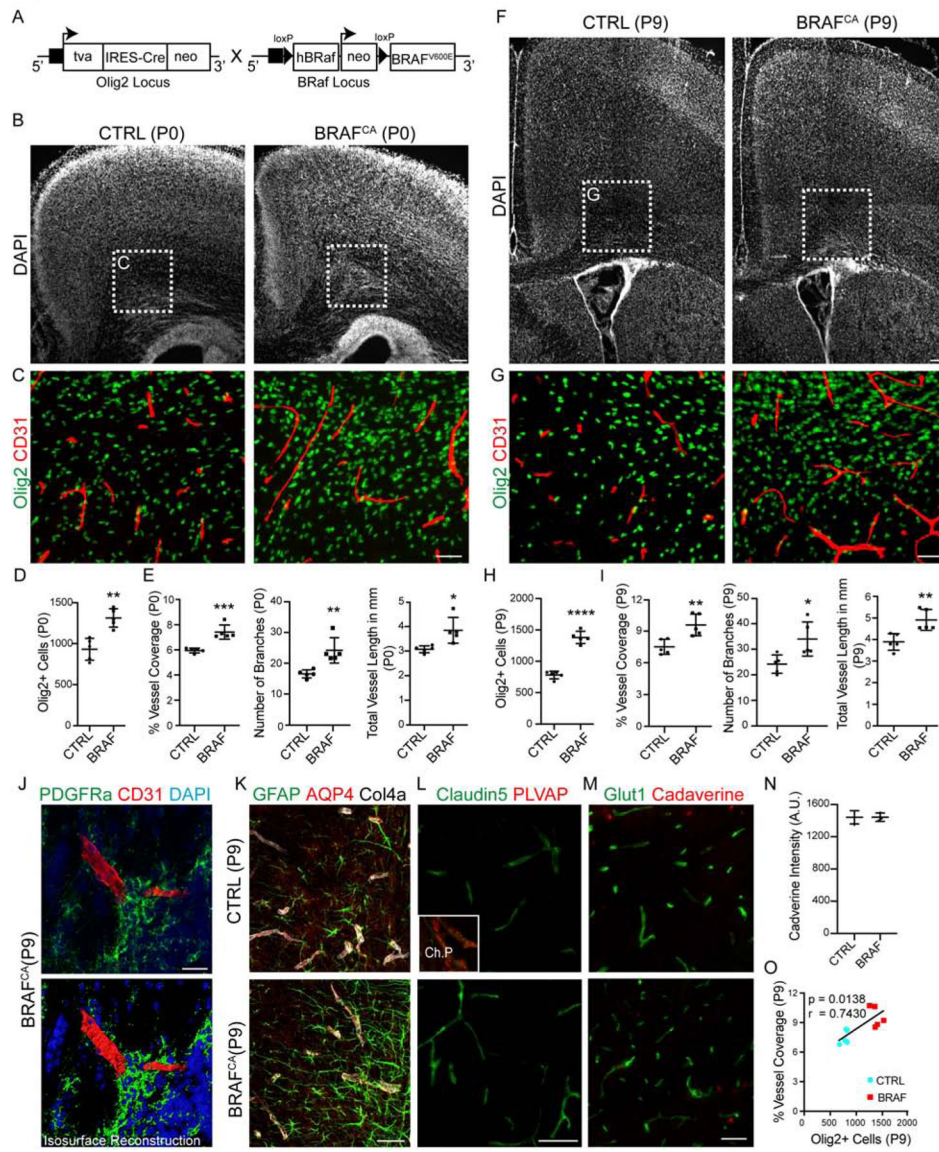


Figure 3: Increased Oligodendroglial Density Induces Hypervascularization of Developing White Matter in $BRAF^{CA}$ Transgenic Mice

(A) Genetic strategy for $BRAF^{CA}$ transgenic mouse generation.

(B, C) DAPI-stained coronal sections from P0 - CTRL and $BRAF^{CA}$ mutant mouse brains.

While $BRAF^{CA}$ mutants do not show any defects in cortical or WM cytoarchitecture, high magnification images of cingulum region (highlighted in C) show increased Olig2+ cells and CD31+ BV density. Scale bars = 100 μ m (B) and 50 μ m (C).

(D, E) Quantification of WM Olig2+ cells in the P0 mice and BV coverage, branching and length in P0 mice.

(F) Forebrain regions in $BRAF^{CA}$ mice appears normal and do not show any neoplasms at P9. DAPI-stained coronal sections from CTRL and $BRAF^{CA}$ brains. Scale bar = 100 μ m

(g) High magnification images from (F) showing sustained increase in Olig2+ oligodendroglial cells and CD31+ BV coverage. Scale bar = 50 μ m.

(H, I) Quantification of WM Olig2+ cells and BV coverage, branching and length in P9 mice.

(J) PDGFRA+ OPCs form clusters on CD31+ BVs in *BRAF^{CA}* mutant WM; (bottom panel) isosurface rendering. Scale bar = 20µm.

(K) Representative images of WM region labelled with GFAP, Aquaporin 4 (AQP4) and Collagen 4a (Col4a) in CTRL and *BRAF^{CA}* mice. Note that no astrocyte endfeet coverage abnormalities were observed. Scale bar = 50µm.

(L) Representative WM images from CTRL and *BRAF^{CA}* brain sections labelled with Claudin 5 and Plasmalemma vesicle protein (PLVAP). Note the absence of Claudin 5 negative and PLVAP positive vessels in WM, indicating no BBB damage. Inset (top) shows choroid plexus vessels from the same section as PLVAP expression positive control. Scale bar = 50µm.

(M, N) Representative WM images from P9 CTRL and *BRAF^{CA}* mice injected with low molecular weight cadaverine-555 tracer injection (Scale bar = 50µm), and intensity quantifications showing no significant changes, *i.e.*, no tracer leakage into brain parenchyma in *BRAF^{CA}* mutants.

(O) Oligodendroglial density and vascular coverage in WM are positively correlated. Data are represented as mean ± S.D. and analyzed by two-tailed unpaired Student's t test. *n*=5 animals/genotype (D–I, O), *n*=3 animals/genotype (N). Significance: **p*<0.05, ***p*<0.01, ****p*<0.001, *****p*<0.0001.

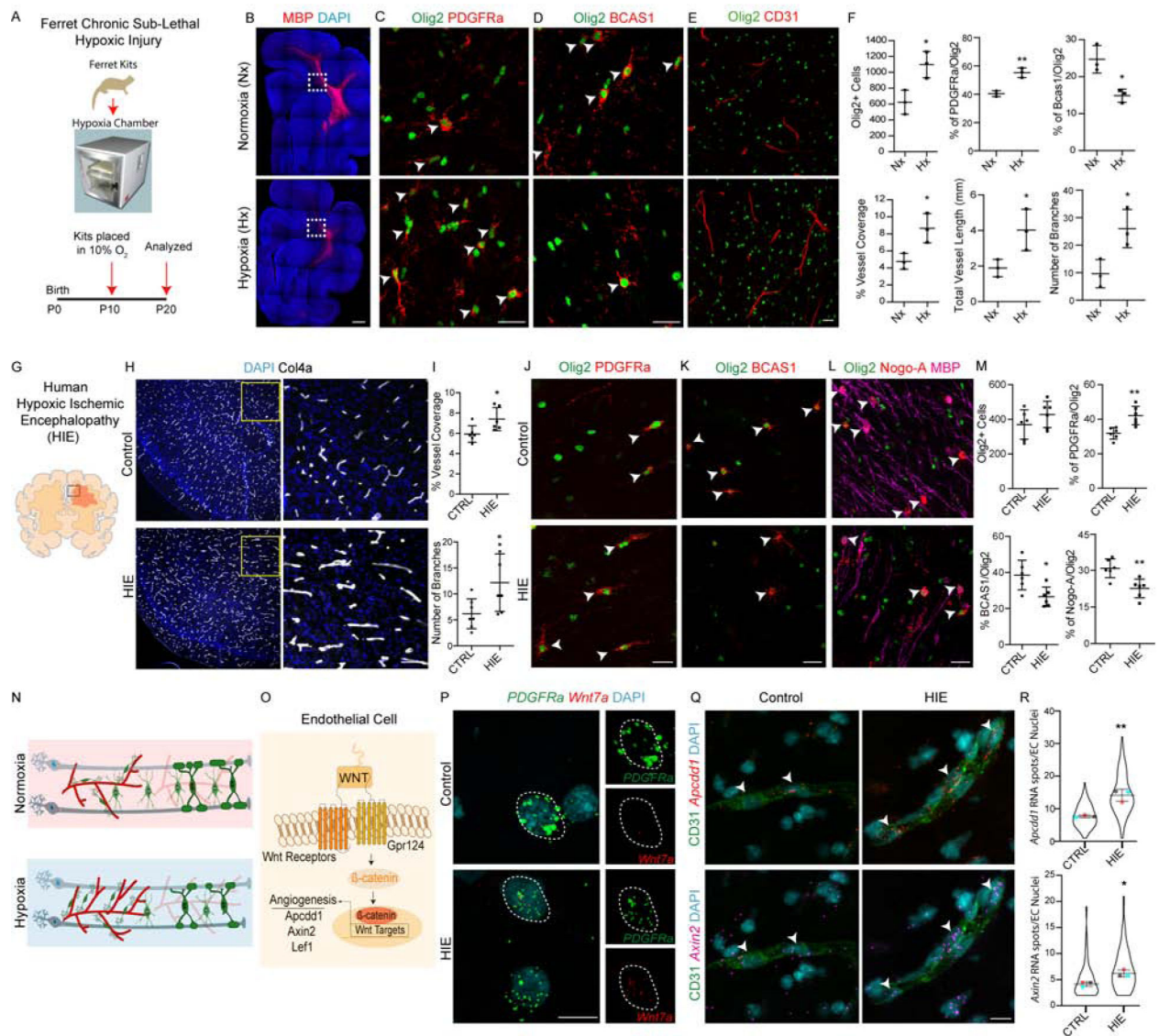


Figure 4: Neonatal White Matter Injury-Induced Increase in Vascular Density is Associated with Increased OPC Number and Upregulated Wnt7 Signaling

(A) Schematic for neonatal ferret chronic sub-lethal hypoxic injury.

(B) Hypomyelination in hypoxic ferret brain. Coronal brain sections from Normoxic (Nx) and Hypoxic (Hx) reared ferret kits stained with myelin basic protein (MBP). Scale bar = 500µm.

(C–D) Increase in PDGFRa+Olig2+ OPCs (C) and decrease in immature BCAS1+Olig2+ immature OLs (D). Scale bars = 25µm.

(E) Increased CD31+ BV coverage in WM of Hx ferrets. Scale bar = 25µm. (F) Quantification of oligodendroglial lineage cells and BV coverage, branching and length in WM tracts of Nx and Hx P20 ferrets.

(G) Cartoon showing WM region in human hypoxic ischemic encephalopathy (HIE). (H) Representative images of WM tracts of cingulate from human HIE and age matched controls

immunostained with BV marker Collagen 4a (Col4a). Note a robust increase in vascular coverage in HIE. Scale bar = 50 μ m.

(I) Quantification of WM vessel features in CTRL and HIE cases.

(J–M) Increase in OPC (PDGFR α +Olig2+; J, M) and decrease in mature OL

(BCAS1+Olig2+ or Nogo-A+Olig2+MBP+; K–M) cell numbers in WM tracts of human HIE cases. Scale bars = 25 μ m.

(N) Cartoon showing hypoxia-induced cellular changes in the WM.

(O) Cartoon of OPC-induced endothelial Wnt signaling.

(P) Multiplex smFISH labelling of *PDGFR α* and *Wnt7a* in CTRL and HIE cases. Scale bar = 10 μ m.

(Q) Multiplex smFISH of Wnt signaling downstream targets *Apcdd1* and *Axin2* and CD31 immunolabelling reveals an increase in EC Wnt signaling in WM tracts of HIE cases. Scale bar = 10 μ m.

(R) Quantification of *Apcdd1* and *Axin2* RNA spots in CD31+ EC nuclei. Data are represented as mean \pm S.D. and analyzed by two-tailed unpaired Student's t test. $n=3$ animals/condition in (F), $n=6$ cases/condition in (I, M) and $n=3$ cases/condition for (R). Violin plots in (R) represent RNA spots quantified from at least 100 cells from 3 different control and HIE cases and overlaying data point represents average number of RNA spots from a single case. Significance: * $p<0.05$, ** $p<0.01$.

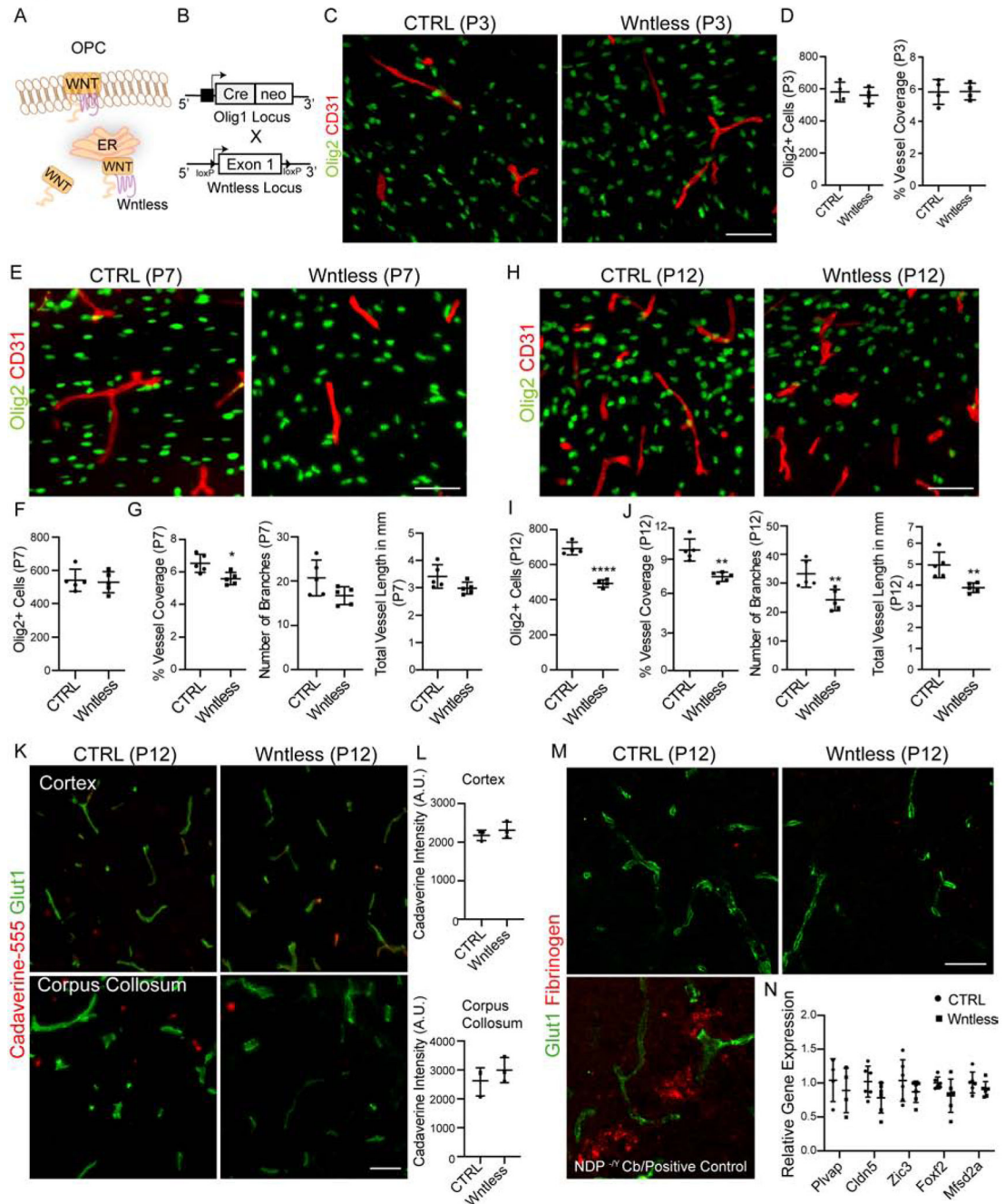


Figure 5: OPC Wnt Activity is Necessary for Postnatal White Matter Vascular Development.

(A) Wntless in the endoplasmic reticulum promotes Wnt ligand production and transport to the plasma membrane where they are secreted.

(B) Schematic of *Wntless* conditional knockout (*Wntless* cKO) generation.

(C, D) White matter BV development in *Wntless* cKO is not affected at P3, as shown by Olig2+ and CD31+ labeling and quantification. Scale bar = 50µm.

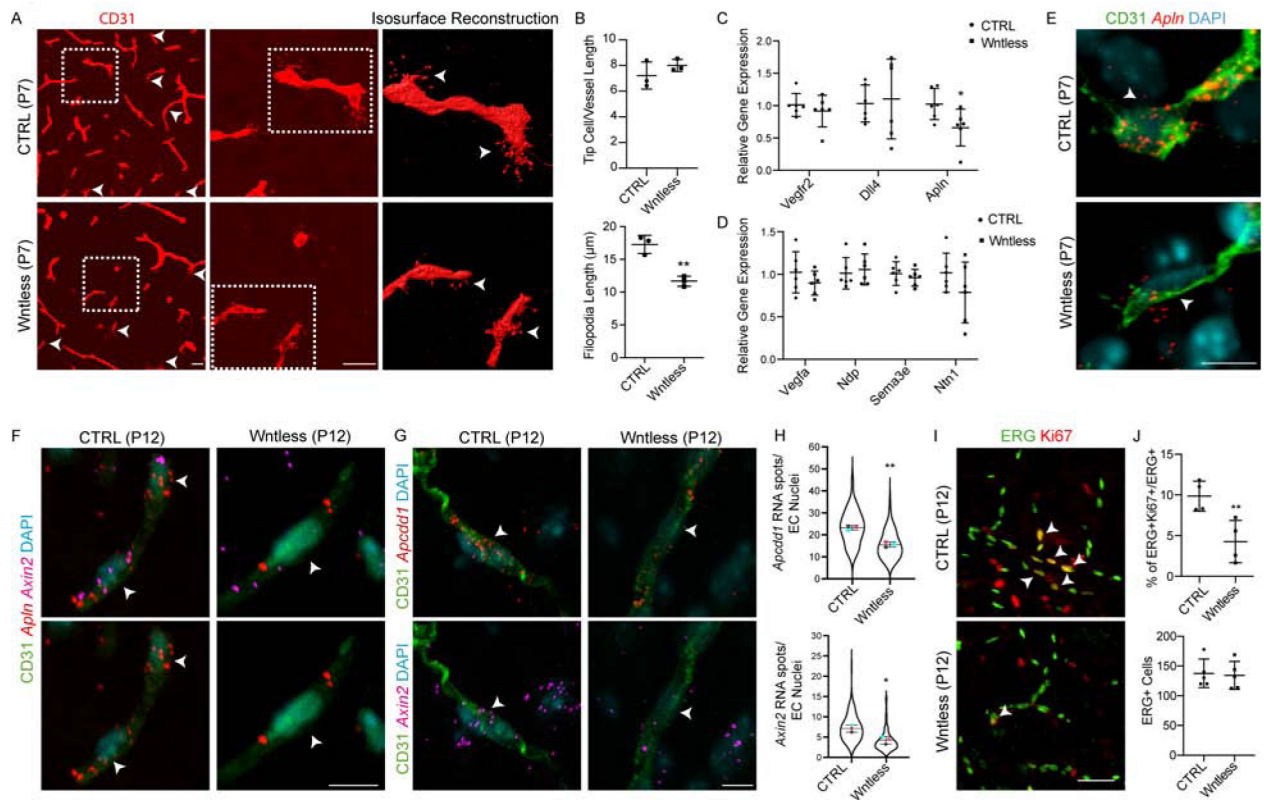
(E–G) Representative images from P7 cortical WM region showing Olig2+ oligodendroglial cells and CD31+ BVs and quantification. Note a decrease in BV density compared to control. Scale bar = 50 μ m.

(H–J) Representative images and quantification from P12 cortical WM showing significantly reduced Olig2+ oligodendroglial cells and CD31+ BV coverage in *Wntless* cKO. Scale bar = 50 μ m.

(K, L) Representative images and quantification of fluorescence intensity from cortex (top panels) and corpus collosum (bottom panels) regions of Cadaverine-555 injected mice reveal no tracer leakage indicating no BBB disruptions in *Wntless* cKO.

(M) Representative images of corpus collosum region from control and *Wntless* cKO mice labelled with Glut1 and Fibrinogen. Note absence of fibrinogen deposits in *Wntless* cKO mice indicating no BBB damage. Bottom left panel shows positive control for fibrinogen staining from cerebellum of *Norrin* (*NDP*^{-Y}) mutants.

(N) qPCR gene expression analysis of WM isolates from CTRL and *Wntless* cKO mice reveals no alterations in expression of genes involved in BBB maturation and maintenance. Data are represented as mean \pm S.D. and analyzed by two-tailed unpaired Student's t test. *n*=4 animals/genotype (D), *n*=6 (F–G), *n*=5 (I–J), *n*=3 (L), *n*=6 (N). Significance: **p*<0.05, ****p*<0.001, *****p*<0.0001.



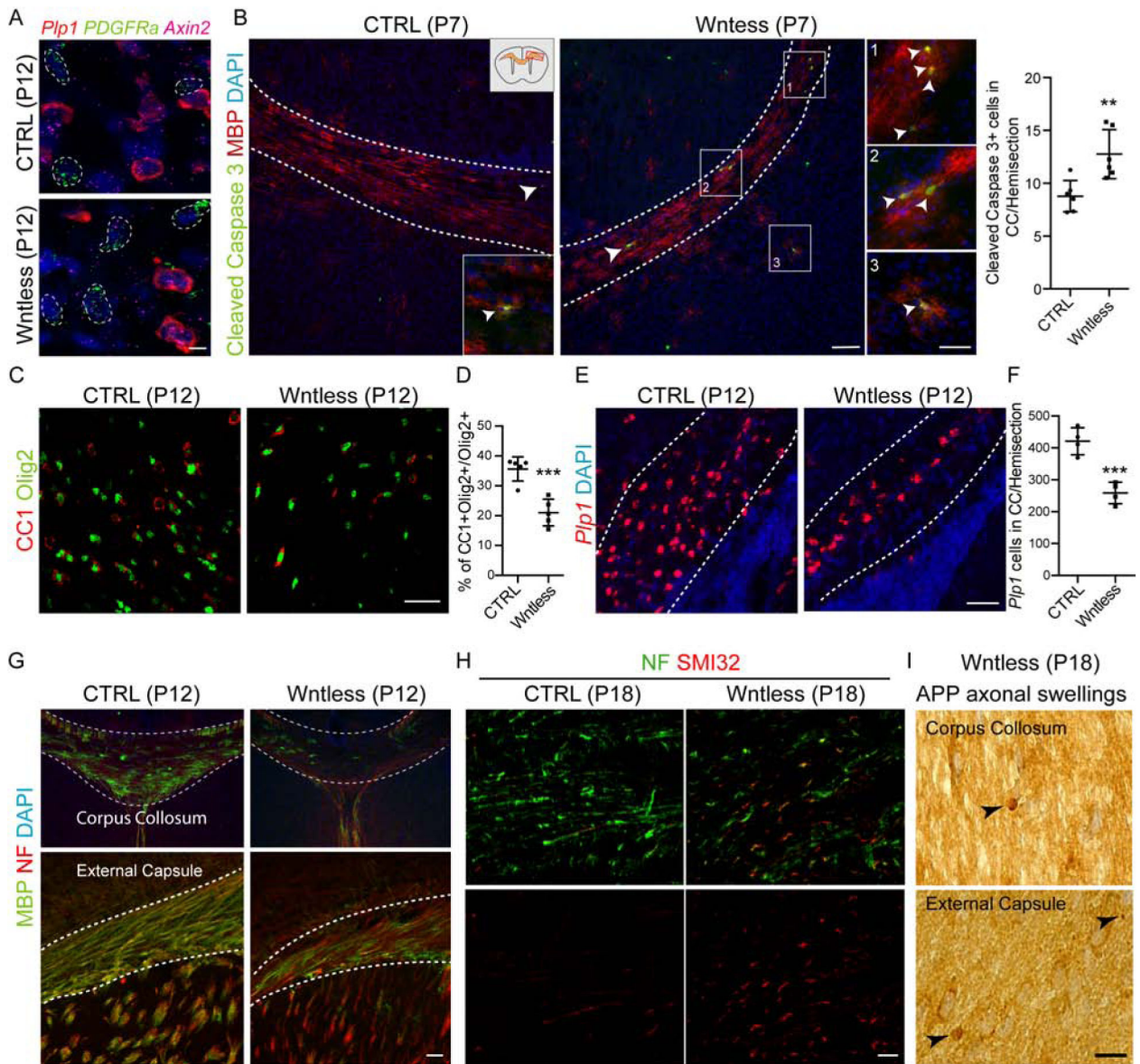


Figure 7: Disruption in Oligodendroglial Intrinsic Wnt ligand Activity Results in Loss of Mature Oligodendrocytes and Hypomyelination.

(A) Multiplex smFISH of *Pip1*, *PDGFRα* and *Axin2* show no alterations in oligodendroglial intrinsic canonical Wnt/ β -catenin activity in *Wntless* cKO mice. *PDGFRα*⁺ OPCs are outlined in white. Scale bar = 5 μ m.

(B) Cortical WM regions labelled with MBP and Cleaved Caspase 3 show increase in OL apoptosis in WM and deep cortex regions in *Wntless* cKO mice at P7. Insets show highlighted regions. Scale bar = 100 μ m and 50 μ m for insets. Right panel shows quantification of Cleaved Caspase 3+ cells in WM.

(C–D) Significant loss of mature OLs (CC1+Olig2+ cells) in *Wntless* cKO animals at P12. Scale bar = 50 μ m.

(E–F) Significant reduction in mature OLs expressing *Pip1* mRNA in *Wntless* cKO at P12. Scale bar = 50 μ m.

(G) Hypomyelination of *Wntless* cKO animals at P12 revealed by myelin basic protein (MBP) and pan-neurofilament marker (NF) immunostaining. Scale bar = 50 μ m. (H) Increase in expression of axonal damage marker SMI32 in the corpus callosum of *Wntless* cKO mice at P18. Scale bar = 10 μ m.

(I) Appearance of amyloid precursor protein (APP+) axonal spheroids in P18 *Wntless* cKO mice (indicated by black arrowheads), indicating axon damage; corpus callosum and external capsule regions are shown. Scale bar = 10 μ m. Data are represented as mean \pm S.D. and analyzed by a two-tailed unpaired Student's t test. $n=6$ animals/genotype for data represented in (B) and $n=5$ and 4 each for data represented in (D) and (F), respectively. Significance: ** $p<0.01$, *** $p<0.001$.

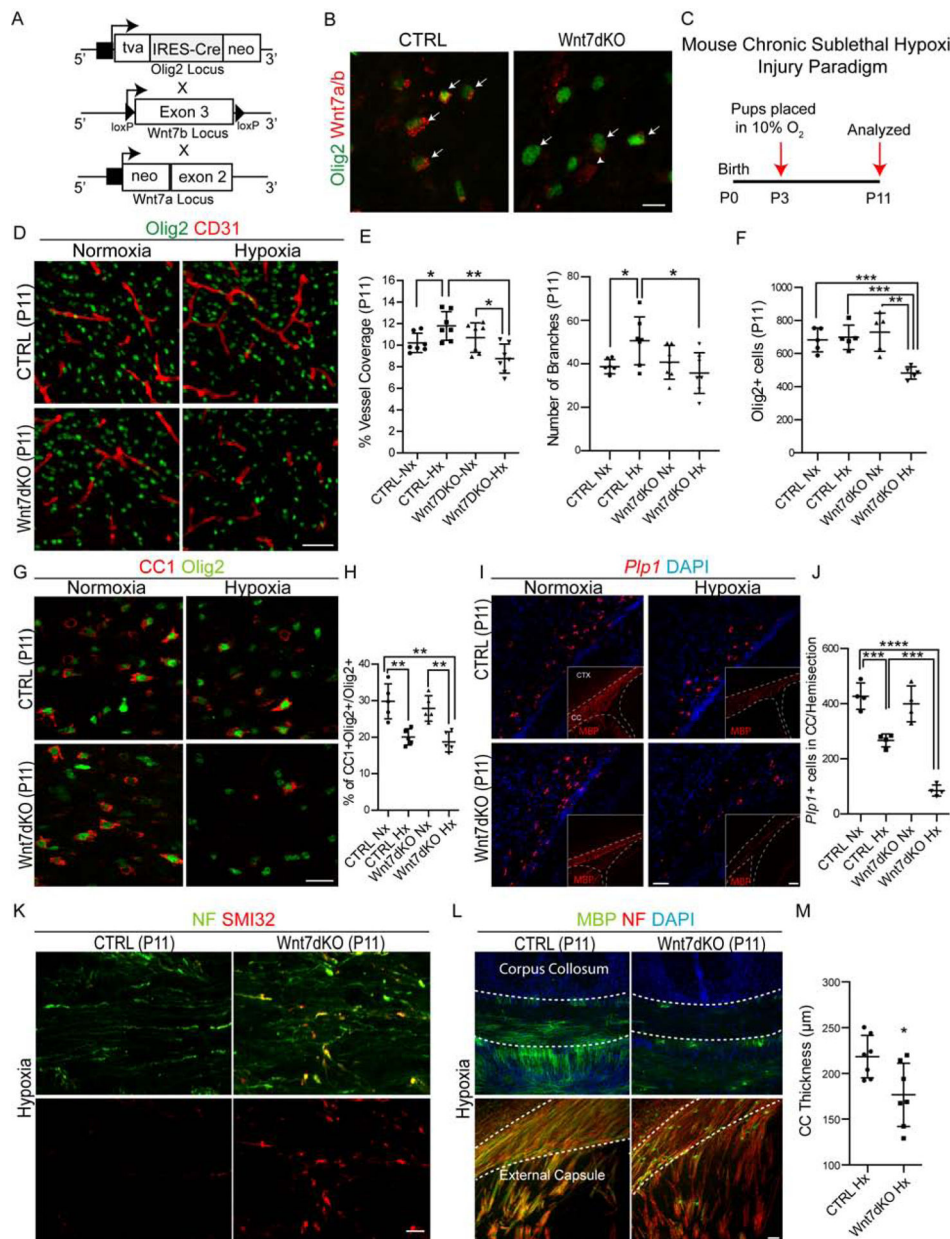


Figure 8: OPC-encoded *Wnt7* Function is Critical for Post Injury Angiogenesis, Myelination and White Matter Integrity.

(A) *Wnt7a/b* double knockout mouse (*Wnt7dKO*) generation strategy.

(B) Immunostaining of *Wnt7a/b* in brain sections at P7 from CTRL and *Wnt7dKO* mice show downregulation of *Wnt7* ligand expression in Olig2+ oligodendroglial cells. Scale bar = 10 μ m.

(C) Schematic for mouse chronic sub-lethal hypoxic injury.

(D–F) Representative images and quantification of Olig2+ oligodendroglial cells and CD31+ BVs from P11 cortical WM region from Nx and Hx reared CTRL and *Wnt7dKO* mice. Note a significant decrease in BV coverage and oligodendroglial cell numbers in Hx mutant versus control. Scale bar = 50 μ m.

(G–H) Loss of CC1+Olig2+ mature oligodendroglial cells in WM region of hypoxic mutants versus control. Scale bar = 25µm.

(I–J) Significant decline in mature OLS expressing *Pip1* mRNA (and MBP protein, inset) in hypoxic *Wnt7dKO* mutants at P11. Scale bars represent 50 µm for (I) and 100 µm for images in insets.

(K) Axonal damage revealed by SMI32 and NF immunostaining in the corpus collosum of hypoxic *Wnt7dKO* animals. Scale bar = 10µm.

(L) Decrease in corpus collosum thickness and axonal myelination in hypoxic *Wnt7dKO* mutants at P11 revealed by MBP and NF immunostaining. Scale bar = 50µm.

(M) Quantification of corpus collosum thickness. Data are represented as mean ± S.D. and analyzed by a two-tailed unpaired Student's t test. $n=7$ animals/genotype and condition for data represented in (D–F, M), $n=5$ for (H) and $n=4$ for (J). Significance: * $p<0.05$,

*** $p<0.001$, **** $p<0.0001$.

KEY RESOURCES TABLE

REAGENT or RESOURCE	SOURCE	IDENTIFIER
Antibodies		
Mouse anti-Olig2	Dr. Charles D. Stiles (Arnett et al., 2004)	RRID: AB_10807410
Goat anti-Olig2	R&D Systems	Cat# AF2418; RRID: AB 2157554
Rabbit anti-CD31/PECAM	ABCAM	Cat# ab28365; RRID: AB 726365
Rat anti-CD31/PECAM	BD Biosciences	Cat# 550274; RRID: AB 393571
Mouse anti-CD31/PECAM	ABCAM	Cat# ab187377, RRID: AB 2756834
Rabbit anti-ERG	Cell Signaling	Cat# 97249, RRID: AB 2721841
Rabbit anti-PDGFRa	Cell Signaling	Cat# 3164, RRID: AB 2162351
Goat anti-Collagen 4a	Millipore	Cat# ab769; RRID: AB 92262
Rabbit anti-Iba1	Wako	Cat# 019-19741; RRID: AB_839504
Mouse anti-Claudin 5	Thermo Fisher Scientific	Cat# 35-2500, RRID: AB_2533200
Chicken anti-GFP	Aves Labs	GFP-1020; RRID: AB_10000240
Rabbit anti-Aquaporin-4	Sigma Aldrich	Cat# A5971; RRID: AB_258270
Rabbit anti-Glut1	Millipore	Cat# 07-1401, RRID: AB_1587074
Rat anti-PLVAP (MECA-32)	BD Biosciences	Cat# ab118533; RRID: AB_10900171
Sheep anti-Fibrinogen	ABCAM	Cat# ab118533; RRID: AB_10900171
Mouse anti-APC (CC-1)	Millipore	Cat# OP80; RRID: AB_2057371
Rat anti-GFAP (2.2B10)	Invitrogen	Cat# 13-0300, RRID: AB_2532994
Mouse anti-BCAS1	Santa Cruz	Cat# sc-136342, RRID: AB_10839529
Mouse anti-Nogo-A	R&D Systems	MAB3098, RRID: AB 10997139
Rat anti-MBP	Millipore	Cat# MAB386, RRID: AB 94975
Rabbit anti-Cleaved Caspase 3	Cell Signaling	Cat# 9661, RRID: AB_2341188
Goat anti-Wnt7	Santa Cruz	Cat# sc-26361; RRID: AB_2215743
Mouse anti-CD68	BD Biosciences	Cat# 556059, RRID: AB_396329
Mouse anti-Ki67	BD Biosciences	Cat# 550609, RRID: AB_393778
Rabbit anti-Lef1	Cell Signaling	Cat# 2230; RRID: AB_823558
Mouse anti-SMI32 (Nonphosphorylated NF-H)	Biologend	Cat# 801702, RRID: AB_2715852
Chicken anti-Neurofilament H	Encor Biosciences	Cat# CPCA-NF-H, RRID: AB_2149761
Mouse anti-APP (A4)	Millipore	MAB348, RRID: AB 94882
Mouse anti-TCF4	Millipore	Cat# 05-511, RRID: AB_309772
Donkey Anti-mouse IgG (H+L), Alexa Fluor 488, 555, 647	Thermo Fisher Scientific	Cat# A-21202; RRID: AB_141607, # A-31570, RRID: AB_2536180, # A-31571, RRID: AB_162542
Donkey Anti-Rabbit IgG (H+L) Antibody, Alexa Fluor 488, 555, 647	Thermo Fisher Scientific	Cat# A-21206; RRID: AB_2535792, # A-31572, RRID: AB_162543, A-31573, RRID: AB_2536183
Donkey Anti-Goat IgG (H+L), Alexa Fluor 488, 594, 647	Thermo Fisher Scientific	Cat# A-11055, RRID: AB_2534102, A-21432, RRID: AB_2535853, A-21447, RRID: AB 2535864

REAGENT or RESOURCE	SOURCE	IDENTIFIER
Goat anti-Chicken IgY (H+L) Secondary Antibody, Alexa Fluor 594	Thermo Fisher Scientific	Cat# A-11042; RRID: AB_2534099
Goat anti-rabbit IgG (H+L) secondary antibody, Alexa fluor 488,555,647	Thermo Fisher Scientific	Cat# A-11008; RRID: AB_143165, # A-21428; RRID: AB_2535849, A-21244; RRID: AB_2535812
Rabbit anti-Olig2	Millipore	Cat# AB9610; RRID: AB_570666
Goat anti-Rabbit IgG Gold (H&L) Ultra Small	Aurion	SKU: 800.011
Biological Samples J		
Postmortem human neonatal brain specimen (See Table S1)	UCSF Pediatric Neuropathology Research Laboratory	N/A
Chemicals, Peptides, and Recombinant Proteins		
SuperScript IV First-Strand Synthesis System	Thermo Fischer Scientific	Cat# 18091050
LightCycler 480 SYBR Green I Master mix	Roche	Cat# 04707516001
RNAScope PDGFRa-Hs Probe	ACD Bio	Cat# 604481-C2
RNAScope Olig2-Hs Probe	ACD Bio	Cat# 424191-C3
RNAScope Wnt7a-Hs Probe	ACD Bio	Cat# 408231-C1
RNAScope Apccdd1-Hs Probe	ACD Bio	Cat# 535851-C2
RNAScope Axin2-Hs Probe	ACD Bio	Cat# 400241-C3
RNAScope PDGFRa-Mm Probe	ACD Bio	Cat# 480661-C2
RNAScope Apccdd1-Mm Probe	ACD Bio	Cat# 425701-C1
RNAScope Axin2-Mm Probe	ACD Bio	Cat# 400331-C3
RNAScope Plp1-Mm Probe	ACD Bio	Cat# 428181-C1
RNAScope Apln-Mm Probe	ACD Bio	Cat# 415371-C1
ProLong gold abtiffade reagent with DAPI	Life Technologies	Cat# P36931
Paraformaldehyde	Thermo Fisher Scientific	Cat# T353-500
Critical Commercial Assays		
RNeasy Mini kit	QIAGEN	Cat# 74104
RNAScope Multiplex Fluorescent Assay Kit	ACD Bio	Cat# 320850
Alexa Fluor™ 555 Cadaverine	Thermo Fisher Scientific	Cat# A30677
Experimental Models: Organisms/Strains		
Sox10-lox-GFP-STOP-lox-DTA	Dr. William Richardson (Kessaris et al., 2006)	N/A
B6.129P2(Cg)-Braf ^{tm1} Mmcm/J	The Jackson Laboratory	RRID: IMSR_JAX:017837
129S-Wlstm 1. 1 Lan/J	The Jackson Laboratory	RRID: IMSR_JAX:012888
B6; 129S1-Wnt7atm 1 Amc/J	The Jackson Laboratory	RRID: IMSR_JAX:004715
B6; 129X1-Wnt7btm2Amc/J	The Jackson Laboratory	RRID: IMSR_JAX:008467
Olig2tm2(TVA,cre)Rth/J	The Jackson Laboratory	RRID: IMSR_JAX:011103
B6; 129S4-Olig1tm 1 (cre) Rth	The Jackson Laboratory	RRID: IMSR_JAX:011105
Oligonucleotides		
For RT-qPCR primers see Table S2	This Study	N/A

REAGENT or RESOURCE	SOURCE	IDENTIFIER
Software and Algorithms		
Image J	National Institutes of Health	RRID: SCR_003070 https://fiji.sc/ or https://imagej.nih.gov/ij/
GraphPad Prism 6	GraphPad Software	RRID: SCR_002798 https://www.graphpad.com/scientific-software/prism/

Author Manuscript

Author Manuscript

Author Manuscript

Author Manuscript